# PERIODIC SOLUTIONS IN THRESHOLD-LINEAR NETWORKS AND THEIR ENTRAINMENT*

ANDREA BEL†, ROMINA COBIAGA‡, WALTER REARTES‡, AND HORACIO G. ROTSTEIN§

**Abstract.** Threshold-linear networks (TLNs) are recurrent networks where the dynamics are threshold-linear (linearly rectified at zero). Mathematically, they consist of coupled non-smooth ordinary differential equations. When the nodes in the network are assumed to be neurons or neuronal populations, TLNs represent firing rate models. We investigate the dynamics of a subclass of TLNs referred to as competitive TLNs where all the connections between different nodes are inhibitory. We prove the existence of periodic solutions in competitive TLNs with three nodes using a combination of mathematical analysis and numerical simulations. We calculate the analytical expressions of the periodic solutions, then we consider a reduced system of transcendental equations and apply a Kantorovich's convergence result to demonstrate the existence of these solutions. We then analyze the attributes (frequency and amplitude) of these periodic solutions as the model parameters vary. Finally, we study the entrainment properties of competitive TLNs in the oscillatory regime, by examining their response to external periodic inputs to one of the nodes in the network. We numerically determine the ranges of input amplitudes and frequencies for which competitive TLNs are able to follow the periodic input for three-node networks and larger networks with cyclic symmetry.

**Key words.** recurrent neural networks, non-smooth dynamical systems, periodic solutions

**AMS subject classifications.** 37N25, 34C25

## 1. Introduction.

Threshold-linear network (TLN) models describe the activity of connected nodes where the input to each cell in the network is a linear combination of the contribution of the other cells when this linear combination is above zero and zero otherwise. In their simplest description, the dynamics of the individual nodes are one-dimensional and linear. When the nodes in the network are neurons or neuronal populations, their activity is interpreted as their firing rate, and the TLNs represent firing rate models [11, 13, 32].

Linear networks (linear node dynamics and linear connectivity) produce relatively simple dynamics where, in particular, sustained network oscillations are excluded. The TLNs we use here (nonlinear connectivity and linear node dynamics) are arguably the simplest nonlinear extension of linear networks that, despite their simplicity, are able to produce complex dynamics including multistability, periodic, quasiperiodic and chaotic temporal patterns, even when the number of nodes in the network is relatively small (e.g., three) [16, 24, 25].

The systematic mathematical study of TLNs has primarily focused on the existence and stability of fixed-points for symmetric TLNs [7, 8, 15] and non-symmetric competitive threshold-linear networks [9, 10, 25]. Competitive TLNs are a specific class of recurrent TLNs where all connectivity weights are negative and there are no

*

†Departamento de Matemática, Universidad Nacional del Sur, Av. Alem 1253, 8000 Bahía Blanca, Buenos Aires, Argentina – INMABB, CONICET, Bahía Blanca, Buenos Aires, Argentina (andrea.bel@uns.edu.ar).

‡Departamento de Matemática, Universidad Nacional del Sur, Av. Alem 1253, 8000 Bahía Blanca, Buenos Aires, Argentina.

§Federated Department of Biological Sciences, New Jersey Institute of Technology and Rutgers University, Newark, NJ. Institute for Brain and Neuroscience Research , New Jersey Institute of Technology , Newark, NJ. Graduate Faculty, Behavioral Neurosciences Program, Rutgers University. Corresponding Investigator, CONICET, Argentina.

self-connections. Inhibitory networks arise in many neuronal systems and have been shown to underlie the generation of rhythmic activity in cognition and motor behavior [1, 3, 18, 21, 22, 28, 31]. Recent modeling work, primarily based on numerical simulations has showed that competitive TLNs with three or more nodes can show very rich dynamics, in particular limit cycle oscillations [9, 24, 25]. However, the existence of periodic solutions in competitive TLNs and their relationship with the networks' fixed-points has not been rigorously discussed.

The goal of this paper is to analyze the existence of periodic solutions to competitive TLNs and their response to periodic inputs. For the specific model investigated in [25] where the periodic solutions were first observed we prove the existence of the limit cycle. This specific case describes the particular situation where the three nodes receive the same constant input. We combine a detailed mathematical analysis with numerical simulations. Our investigation is based on the theory of non-smooth dynamical systems [12, 30]. We first carry out a bifurcation analysis that allows us to formulate a hypothesis for the existence of periodic solutions in the network as a function of the inputs to the participating nodes. Then, we calculate the analytical expressions for the periodic solutions and prove their existence by considering the solutions to a reduced system of equations associated to these analytical expressions. We subsequently study the dependence of periodic solutions with the model parameters. Finally, we analyze the response of competitive TLNs to periodic inputs applied to one of the participating nodes. We begin our study with three-node networks and then extend it to networks with a larger number of nodes and cyclic symmetry.

The overview of the paper is as follows. In Section 2, we describe the three-node competitive TLN. We review some basic results about the model equilibria and their stability, and we compute and classify all bifurcations of these equilibria, which are the basis for the cycle generation analysis presented in the following sections. In Section 3, we study the existence of periodic solutions with small amplitude: we calculate the analytical expression of these periodic solutions and analyze their stability. We also describe a reduced system of transcendental equations whose solutions are in correspondence with the limit cycles of the network, and use it to prove the existence of limit cycles for different values of the parameters. In Section 4, we describe how the periodic solutions of the network are affected by changes in the values of the constant input of the nodes or the connection strength connections between nodes. In Section 5, we consider three-node networks in which oscillatory solutions are observed. We assume that an external sinusoidal input is added to one of the nodes and, by defining a Poincaré map, we numerically determine whether and how the oscillatory solutions are modified by this periodic input. Finally, in Section 6 we extend the previous work to competitive TLNs having three or more nodes, all-to-all connections and cyclic symmetry. Following the techniques used in Section 3, we find the analytical expressions of the oscillatory solutions. Then, we study the cycle attributes when either the number of nodes or the parameter values vary, and we briefly analyze the response of the network as an external sinusoidal input is added to one of the nodes. We discuss our results in Section 7.

## 2. Three-node network: equilibria and bifurcations.

In this section we describe the threshold-linear network that we will study in the following three sections. We first present some basic results about the model equilibria and their stability. Then, we calculate and classify all bifurcations of equilibria which are the basis for the cycle generation analysis presented in Section 3.

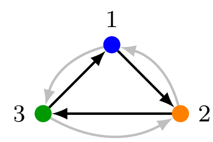


FIG. 1. *Graph representation of a three-node network where a black arrow indicates weak inhibition, whereas a gray arrow indicates strong inhibition between nodes.*

We consider a non-smooth network with three nodes described by

$$\frac{dx_i}{dt} = -x_i + \left[\sum_{j=1}^{3} W_{ij} x_j + \theta_i\right]_+ , \qquad i = 1, 2, 3, \tag{2.1}$$

where $x_i$ is the level of activity of node $i$ (the firing rate), $W_{ij}$ represents the strength of the connection from node $j$ to node $i$, $\theta_i > 0$ is a constant input and $[\cdot]_+$ is the threshold-linear function defined by $[y]_+ = \max(0, y)$.

We assume that $W_{ii} = 0$ for all $i$ (so for each node self-inhibition results only from the second term on the left-hand side of (2.1)). In addition, we assume that all connections between nodes are inhibitory, that is, $W_{ij} < 0$, for $1 \le i, j \le 3$, $i \ne j$. We follow the assumptions in [25] and consider the action of a strong global inhibition term (constant for all connectivity weights), which is added to the local connections between nodes. If the local connection is inhibitory (excitatory), it is said that the resulting inhibition is strong (weak). Therefore, even if the local connectivity is excitatory, the effect of the global inhibition may cause the network to be a competitive TLN. Also, following [25], we use $-1-\delta$, with $\delta > 0$, for strong inhibition, and $-1+\epsilon$, with $0 < \epsilon < 1$, for weak inhibition. Because all the non-zero connectivity weights are negative, it can be proved easily that the activity of node $i$ is bounded, moreover the activity $x_i$ remains in $[0, \theta_i]$ provided the initial conditions belong to that interval [4, 25].

The connectivity matrix for the three-node network we use is given by

$$W = \begin{bmatrix} 0 & -1-\delta & -1+\epsilon \\ -1+\epsilon & 0 & -1-\delta \\ -1-\delta & -1+\epsilon & 0 \end{bmatrix} = \begin{bmatrix} 0 & -1 & -1 \\ -1 & 0 & -1 \\ -1 & -1 & 0 \end{bmatrix} + \begin{bmatrix} 0 & -\delta & \epsilon \\ \epsilon & 0 & -\delta \\ -\delta & \epsilon & 0 \end{bmatrix}, \tag{2.2}$$

and the network has the graph representation showed in Figure 1.

The network (2.1)-(2.2) is the smallest one in which oscillatory activity has been observed [25]. In their simulations they used $\theta_i = 1$ for all nodes. Two-node competitive TLNs are not expected to exhibit periodic oscillations since a mechanism of amplification accompanying the negative feedback necessary for sustained oscillatory activity is lacking. In three-node networks this mechanism can be provided by disinhibition ("inhibition of inhibition"). Below we describe these oscillatory solutions. To simplify the calculations and for the sake of clarity we consider that two nodes of the network have the same fixed constant input ($\theta_1 = \theta_2 = \theta$) and the other node has an arbitrary positive input ($\theta_3$). The general case can be analyzed with similar techniques. Defining $\mu = \theta_3/\theta$ and rescaling the variables (by the factor $1/\theta$), we obtain the system

$$\frac{d\mathbf{x}}{dt} + \mathbf{x} = [\, W\mathbf{x} + B \,]_+ , \tag{2.3}$$

with $W$ defined in (2.2) and $B = [1, 1, \mu]^T$.

In the rest of the present section we consider the system (2.3), and we perform a dynamical system analysis for the bifurcation parameter $\mu$ and the auxiliary parameters $\delta$ and $\epsilon$.

**2.1. Equilibria and their stability.** We begin the study of the network (2.3) by calculating the equilibria as functions of the model parameters. These equilibria are the solutions of

$$x_i = [f_i(x_1, x_2, x_3)]_+, \quad i = 1, 2, 3. \tag{2.4}$$

where we define $f_i : \mathbb{R}^3 \to \mathbb{R}$ for $i = 1, 2, 3$, as

$$f_i(x_1, x_2, x_3) = \sum_{j=1}^{3} W_{ij} x_j + 1, \quad i = 1, 2, \qquad f_3(x_1, x_2, x_3) = \sum_{j=1}^{3} W_{3j} x_j + \mu. \tag{2.5}$$

System (2.4) is piecewise linear and its solutions depend on the values of the functions $f_i$. To clear up the calculations we define the transition planes (or, in the general case, transition hyperplanes)

$$\Sigma_i = \{\mathbf{x} \in \mathbb{R}^3 : f_i(x) = 0\}, \qquad i = 1, 2, 3, \tag{2.6}$$

and the following seven regions in $\mathbb{R}^3$

$$\begin{aligned} S_{123} &= \{\mathbf{x} \in \mathbb{R}^3 : f_i(x) > 0, \, \forall\, i\}, \\ S_{ij} &= \{\mathbf{x} \in \mathbb{R}^3 : f_{i,j}(x) > 0 \;\wedge\; f_k(x) < 0, \;\; k \neq i, j\}, \quad 1 \leq i < j \leq 3, \\ S_i &= \{\mathbf{x} \in \mathbb{R}^3 : f_i(x) > 0 \;\wedge\; f_{j,k}(x) < 0, \;\; j, k \neq i\}, \quad i = 1, 2, 3. \end{aligned} \tag{2.7}$$

Each region contains, at most, one solution of (2.4), that is, one equilibrium of (2.3).

To calculate the equilibrium (if it exists within the region of interest) and its stability properties we use the corresponding linear system. For example, in the $S_{123}$ region, the equation (2.4) results $\mathbf{x} = W\mathbf{x} + B$. In this case the equilibrium has the form $\mathbf{x}^* = (I - W)^{-1} B$, provided that $I - W$ is invertible and $\mathbf{x}^* \in S_{123}$. It's stability properties are analyzed by computing the eigenvalues of $W - I$.

These equilibria are:

$$\begin{aligned} \mathbf{x}^*_{123} &= d_1[\epsilon^2 + \delta\epsilon + \delta^2\mu + (2\delta + \epsilon)(\mu - 1), \delta^2 + \delta\epsilon + \epsilon^2\mu - (2\epsilon + \delta)(\mu - 1), \\ &\qquad \delta^2 + \epsilon^2 + \delta\epsilon\mu + (\epsilon - \delta)(\mu - 1)]^T, \\ \mathbf{x}^*_{13} &= d_2[1 + (\epsilon - 1)\mu, 0, -(1 + \delta) + \mu]^T, \\ \mathbf{x}^*_{23} &= d_2[0, 1 - (1 + \delta)\mu, \epsilon - 1 + \mu]^T, \\ \mathbf{x}^*_{2} &= [0, 1, 0]^T, \qquad \mathbf{x}^*_{3} = [0, 0, \mu]^T, \end{aligned} \tag{2.8}$$

with $d_1 = ((3 + \delta - \epsilon)(\delta^2 + \delta\epsilon + \epsilon^2))^{-1}$ and $d_2 = (-\delta + (\delta + 1)\epsilon)^{-1}$, and where the subscript indicates the region to which they belong. We note that while the underlying linear system may posses an equilibrium, this may be located outside the region we are analyzing (region of interest). We observe that in two cases, specifically for the regions $S_{12}$ and $S_1$, the equilibria for the corresponding linear system do not belong to the region for any value of the parameters $\delta$, $\epsilon$ and $\mu$, and therefore we do not include them in (2.8).

The equilibrium in $S_{123}$ is an unstable (stable) focus if $\epsilon < \delta$ ($\epsilon > \delta$). The equilibria in the $S_{ij}$ regions are saddle points if $0 < \epsilon < \delta/(1 + \delta)$, whereas they are

| $\epsilon$ \ $\mu$ | $(0, c_1)$ | $(c_1, c_3)$ | $(c_3, c_4)$ | $(c_4, c_2)$ | $(c_2, \infty)$ |
|---|---|---|---|---|---|
| $\left(0, \frac{\delta}{1+\delta}\right)$ | $\mathbf{x}_2^*$ (s) | $\mathbf{x}_2^*$ (s)<br>$\mathbf{x}_{23}^*$ (u)<br>$\mathbf{x}_{123}^*$ (u) | $\mathbf{x}_{123}^*$ (u) | $\mathbf{x}_3^*$ (s)<br>$\mathbf{x}_{13}^*$ (u)<br>$\mathbf{x}_{123}^*$ (u) | $\mathbf{x}_3^*$ (s) |

| $\epsilon$ \ $\mu$ | $(0, c_3)$ | $(c_3, c_1)$ | $(c_1, c_2)$ | $(c_2, c_4)$ | $(c_4, \infty)$ |
|---|---|---|---|---|---|
| $\left(\frac{\delta}{1+\delta}, 1\right)$ | $\mathbf{x}_2^*$ (s) | $\mathbf{x}_{23}^*$ (s) | $\mathbf{x}_{123}^*$ (u) if $\epsilon < \delta$<br>(s) if $\epsilon > \delta$ | $\mathbf{x}_{13}^*$ (s) | $\mathbf{x}_3^*$ (s) |

TABLE 1

*Non-boundary equilibria of system (2.3) given in (2.8). For each equilibrium we indicate its stability depending on the values of the parameters: (s) stable and (u) unstable. The critical values $c_i$ are given in (2.9).*

stable nodes if $\delta/(1+\delta) < \epsilon < 1$. Finally, the equilibria in the $S_i$ regions are stable nodes since the linear matrices of the corresponding systems have a triple eigenvalue $-1$. In Table 1 we summarize the information about the equilibria of system (2.3).

We calculate the critical values of the parameter $\mu$ by solving the equations $f_i(\mathbf{x}^*) = 0$ for the equilibria in (2.8). We obtain four critical values of $\mu$ given by

$$(2.9) \quad c_1 = \frac{2\delta - \delta\epsilon + \epsilon - \epsilon^2}{\delta^2 + 2\delta + \epsilon}, \quad c_2 = \frac{\delta^2 + \delta + \delta\epsilon + 2\epsilon}{\delta + 2\epsilon - \epsilon^2}, \quad c_3 = (1-\epsilon), \quad c_4 = \frac{1}{1-\epsilon},$$

which verify the relations $c_1 < c_2$ and $c_3 < c_4$, for all values of the parameters $\delta > 0$ and $0 < \epsilon < 1$. For these critical values, system (2.3) has boundary equilibria (i.e., equilibria in one of the transition planes $\Sigma_i$). In the following subsection we study the equilibrium bifurcations associated with the boundary equilibria in our system.

*Remark* 2.1. If $\epsilon = \delta/(\delta+1)$, the equilibria in regions $S_{23}$ and $S_{13}$ are non-hyperbolic. If $\epsilon = \delta$ the equilibrium $\mathbf{x}_{123}^* \in S_{123}$ is a linear center, i.e., a family of periodic solutions exists surrounding the equilibrium $\mathbf{x}_{123}^*$.

As an example, in Figure 2 we show one of the possible configurations of the equilibria as the parameter $\mu$ varies. There are different branches of equilibria connected at the critical values of $\mu$ given in (2.9). These values of the parameter are associated with bifurcations of the system (2.3). In the following subsections we describe the different equilibrium bifurcations and how they are related to the generation of periodic solutions.

**2.2. Boundary equilibrium bifurcations.** In non-smooth continuous systems, a boundary equilibrium bifurcation occurs if (i) there is a boundary equilibrium (in a transition plane) at a critical value of the parameter, and (ii) certain non-degeneracy conditions are satisfied [12, 30]. There are two possible universal unfoldings of this bifurcation. In one of them, called a persistent (or border-crossing) scenario, when the parameter varies, a branch of equilibria lying in one region transitions into another branch of equilibria lying in other region. The other universal unfolding is the non-smooth fold scenario. In this bifurcation, when the parameter varies, two branches of equilibria collide at the boundary equilibrium and then disappear. For a $n$-dimensional system with only one transition variety, analytical conditions exist for distinguishing between the above two cases [12]. Applying this theory we obtain the following result describing all boundary equilibrium bifurcations for our model.

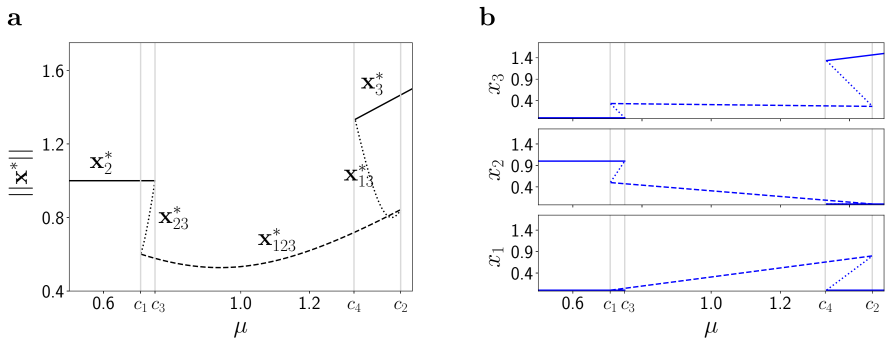


FIG. 2. *Equilibria as functions of parameter $\mu$ for the fixed values $\delta = 1/2$ and $\epsilon = 1/4$. The different types of lines correspond to different branches of equilibria. Stable (unstable) equilibria are indicated in solid (dashed and dotted) line. The vertical gray lines correspond to the critical values $c_i$ defined in* (2.9)*.* **a.** *Norm $||\mathbf{x}^*||$ of the equilibria indicated in labels.* **b.** *Coordinates of the equilibria in* **a***.*

THEOREM 2.2. *For fixed values of $\delta$ and $\epsilon$, if $\epsilon \neq \delta/(1+\delta)$, the system* (2.3) *has a boundary equilibrium bifurcation at each critical value $\mu = c_i$ defined in* (2.9) *for $i = 1, \ldots, 4$. In all cases the bifurcation is a non-smooth fold if $0 < \epsilon < \delta/(1+\delta)$, and it is a persistent bifurcation if $\delta/(1+\delta) < \epsilon < 1$.*

*Proof.* For $\mu = c_1 = \dfrac{2\delta - \delta\epsilon + \epsilon - \epsilon^2}{\delta^2 + 2\delta + \epsilon}$, the boundary equilibrium of (2.3), $\mathbf{x}^* \in \Sigma_1$, results in

$$\mathbf{x}^* = \left[0, \frac{\delta + \epsilon}{\delta^2 + 2\delta + \epsilon}, \frac{\delta}{\delta^2 + 2\delta + \epsilon}\right]^T. \tag{2.10}$$

In a neighborhood of $\mathbf{x}^*$, by defining the variables $\hat{\mathbf{x}} = \mathbf{x} - \mathbf{x}^*$ and $\hat{\mu} = \mu - c_1$, we express system (2.3) in the translated form

$$\frac{d\hat{\mathbf{x}}}{dt} = \begin{cases} N_0\hat{\mathbf{x}} + M\hat{\mu}, & \text{if} \quad C^T\hat{\mathbf{x}} \geq 0, \\ N_1\hat{\mathbf{x}} + M\hat{\mu} = (N_0 + EC^T)\hat{\mathbf{x}} + M\hat{\mu}, & \text{if} \quad C^T\hat{\mathbf{x}} < 0, \end{cases} \tag{2.11}$$

where $N_0 = \begin{bmatrix} -1 & -1-\delta & -1+\epsilon \\ -1+\epsilon & -1 & -1-\delta \\ -1-\delta & -1+\epsilon & -1 \end{bmatrix}$, $M = \begin{bmatrix} 0 \\ 0 \\ 1 \end{bmatrix}$, $C = \begin{bmatrix} 0 \\ -1-\delta \\ -1+\epsilon \end{bmatrix}$ and $E = [-1, 0, 0]^T$. The condition $C^T\hat{\mathbf{x}} = 0$ corresponds to values of $\mathbf{x} \in \Sigma_1$, and therefore the expression (2.11) represents the linear systems in the regions $S_{123}$ and $S_{23}$ separated by the plane $\Sigma_1$.

For $\hat{\mu} = 0$, the system (2.11) has a boundary equilibrium at the origin. Since $\epsilon \in (0, 1)$ and $\epsilon \neq \delta/(1+\delta)$, it follows that $\det(N_0) \neq 0$, $C^T N_0^{-1} M \neq 0$ and $1 + C^T N_0^{-1} E \neq 0$. Thus, the system (2.11) has a boundary equilibrium bifurcation at the critical value $\hat{\mu} = 0$. Moreover, using standard results [12] (see theorem 5.1 there) the universal unfolding of this bifurcation can be determined by the sign of

$$1 + C^T N_0^{-1} E = \frac{-\delta + (\delta + 1)\epsilon}{(3 + \delta - \epsilon)(\delta^2 + \delta\epsilon + \epsilon^2)}. \tag{2.12}$$

Specifically, if $0 < \epsilon < \delta/(1+\delta)$, we then obtain $1 + C^T N_0^{-1} E < 0$, therefore the system (2.11) has a non-smooth fold bifurcation. If $\delta/(1+\delta) < \epsilon < 1$, we have $1 + C^T N_0^{-1} E > 0$, and the system shows a persistent scenario.

For $\mu = c_2 = \dfrac{\delta^2+\delta+\delta\epsilon+2\epsilon}{\delta+2\epsilon-\epsilon^2}$, the boundary equilibrium $\mathbf{x}^* \in \Sigma_2$ is given by

$$\mathbf{x}^* = \left[\frac{\delta+\epsilon}{\delta+2\epsilon-\epsilon^2}, 0, \frac{\epsilon}{\delta+2\epsilon-\epsilon^2}\right]^T. \tag{2.13}$$

The proof is analogous to the above case with $\hat{\mu} = \mu - c_2$, for the same matrices $N_0$ and $M$, and

$$C = \begin{bmatrix} -1+\epsilon \\ 0 \\ -1-\delta \end{bmatrix}, \quad E = \begin{bmatrix} 0 \\ -1 \\ 0 \end{bmatrix}. \tag{2.14}$$

For $\mu = c_3 = (1-\epsilon)$, the boundary equilibrium results in $\mathbf{x}^* = [0,1,0]^T \in \Sigma_3$. As before, the proof is analogous to the first case considering $\hat{\mu} = \mu - c_3$ and the matrices

$$N_0 = \begin{bmatrix} -1 & 0 & 0 \\ -1+\epsilon & -1 & -1-\delta \\ -1-\delta & -1+\epsilon & -1 \end{bmatrix}, \; C = \begin{bmatrix} -1-\delta \\ -1+\epsilon \\ 0 \end{bmatrix}, \; E = \begin{bmatrix} 0 \\ 0 \\ -1 \end{bmatrix}. \tag{2.15}$$

The system presents a boundary equilibrium bifurcation at $\hat{\mu} = 0$ and $1 + C^T N_0^{-1} E = (-\delta + (\delta+1)\epsilon)^{-1}$, then, from the sing of this constant the conclusions follow directly.

Finally, for $\mu = c_4 = 1/(1-\epsilon)$, the proof is similar to the case $\mu = c_1$ but considering the boundary equilibrium $\mathbf{x}^* = [0,0,\mu]^T \in \Sigma_1$, $\hat{\mu} = \mu - c_4$ and the matrices

$$N_0 = \begin{bmatrix} -1 & -1-\delta & -1+\epsilon \\ 0 & -1 & 0 \\ -1-\delta & -1+\epsilon & -1 \end{bmatrix}, \; C = \begin{bmatrix} 0 \\ -1-\delta \\ -1+\epsilon \end{bmatrix}, \; E = \begin{bmatrix} -1 \\ 0 \\ 0 \end{bmatrix}. \tag{2.16}$$ □

The above theorem indicates the critical values of the parameters for which the system (2.3) has equilibrium bifurcations, but, it does not describe how the branches of equilibria interact for values of the parameter $\mu$ near the critical values. To describe completely the various dynamical scenarios we consider the results in Theorem 2.2 along with the information about the existence and stability of equilibria (see (2.8) and Table 1). We summarize some of these results in the following theorem.

THEOREM 2.3. *In a small neighborhood of the critical values $\mu = c_1$ and $\mu = c_2$ given in (2.9), the system (2.3) has two branches of equilibria (depending on $\mu$) verifying the following.*

- *If $0 < \epsilon < \delta/(1+\delta)$, the system has a non-smooth fold bifurcation at $\mu = c_1$ and $\mu = c_2$. Two equilibria exist for $\mu > c_1$ ($\mu < c_2$): an unstable focus $\mathbf{x}^*_{123}(\mu) \in S_{123}$ and a saddle fixed point $\mathbf{x}^*_{23}(\mu) \in S_{23}$ ($\mathbf{x}^*_{13}(\mu) \in S_{13}$).*
- *If $\delta/(1+\delta) < \epsilon < \delta$, the system shows a persistent scenario at $\mu = c_1$ and $\mu = c_2$. In particular, near the critical value $c_1$, a stable node $\mathbf{x}^*_{23}(\mu) \in S_{23}$ exists for $\mu < c_1$, and an unstable focus $\mathbf{x}^*_{123}(\mu) \in S_{123}$ exists for $\mu > c_1$. Whereas, near the critical value $c_2$, an unstable focus $\mathbf{x}^*_{123}(\mu) \in S_{123}$ exists for $\mu < c_2$, and a stable node $\mathbf{x}^*_{13}(\mu) \in S_{13}$ exists for $\mu > c_2$.*

In the above theorem we only analyze bifurcations involving an unstable focus because they are the equilibria related with the generation of limit cycles as we will show in the next section. In Figure 3 we show the two possible scenarios for the bifurcation at $\mu = c_1$. We consider the fixed value $\delta = 1/2$ and two representative

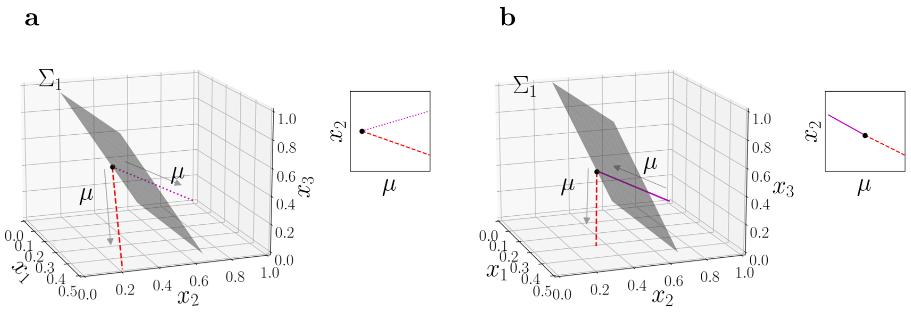


Fig. 3. *Scheme of different bifurcations observed in system* (2.3) *at* $\mu = c_1$. **a.** *Non-smooth fold bifurcation.* **b.** *Persistent bifurcation. We show the transition plane* $\Sigma_1$*, the boundary equilibrium (black dot) and the two branches of equilibria observed when the parameter varies. Stable (unstable) equilibria are indicated in solid (dashed and dotted) line. The inset diagrams show one coordinate of the equilibria as functions of* $\mu$.

values of $\epsilon$. We show a non-smooth fold bifurcation (Fig. 3 a) where both interacting equilibria are unstable and they exist for values of $\mu > c_1$. Also, we show a persistent case (Fig. 3 b) where a stable node is transformed in an unstable focus when the value of $\mu$ is increased.

**3. Cycles generated in boundary equilibrium bifurcations: existence and stability.** In Section 2 we described all boundary equilibrium bifurcations of system (2.3). In particular, we found conditions for the parameters for which the system has bifurcations with one branch of unstable foci. These dynamical scenarios are particularly interesting because the rotational field around the unstable focus allows that trajectories near the transition plane to come back on that plane. This behavior is one of the properties that enable the existence of periodic solutions in the system.

In two dimensional systems the existence of cycles generated in an equilibrium bifurcation can be determined using analytical conditions like the ones presented in [12]. In three dimensional systems only a few results exist for very specific systems, for example, if the two equilibria interacting in the bifurcation are foci (see Chapter 5 of [12]). However, in the general case, the existence of limit cycles and chaotic attractors in piecewise linear three dimensional systems is an open problem.

In this section, we study the existence of periodic solutions related to the boundary equilibrium bifurcations already calculated for the network (2.3). If the amplitude is small enough, we find the analytical expression for the solutions by solving the system in each region separately and adding continuity conditions. Then, we analyze the stability of the cycles and prove their existence for different values of the parameters.

**3.1. Analytical expressions of limit cycles.** If $0 < \epsilon < \delta$ system (2.3) has an unstable focus and shows one of the two different dynamical scenarios showed in the above section (see Figure 3). In both cases, periodic solutions could be generated in the boundary equilibrium bifurcations at the critical values $\mu = c_1$ or $\mu = c_2$. In this subsection we assume that a cycle with small enough amplitude exists and we determine its analytical expression for values of the parameter near these critical values.

Here we consider the critical value $\mu = c_1$, where system (2.3) has the boundary equilibrium $\mathbf{x}^* \in \Sigma_1$ given in (2.10). We define $\hat{\mathbf{x}} = \mathbf{x} - \mathbf{x}^*$, $\hat{\mu} = \mu - c_1$, the transition

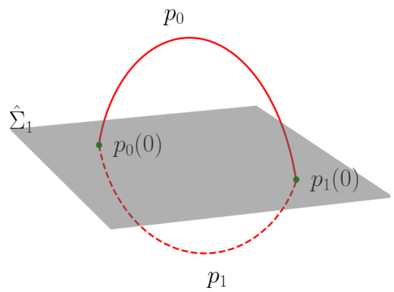


FIG. 4. *A periodic solution crossing the transition plane* $\hat{\Sigma}_1$*. The plane divides the solution in two parts,* $p_0$ *and* $p_1$*. The dots indicate the initial condition* $p_0(0)$ *and* $p_1(0)$*.*

plane $\hat{\Sigma}_1$, and the regions $\hat{S}_{123}$ and $\hat{S}_{23}$ as the translation of the original objects (defined in (2.6) and (2.7)). To analyze the behavior of the solutions to system (2.3) in some neighborhood of the bifurcation value we use the translated system (2.11). From Theorem 2.3 it follows that an unstable focus for (2.3) exists for $\mu > c_1$, therefore an unstable focus for (2.11) exists for $\hat{\mu} > 0$. We emphasize that system (2.11) remains unchanged if we consider $\hat{\mathbf{x}}$ and $\hat{\mu}$ scaled by the same positive value (the system is scale invariant), therefore it is enough to study the case $\hat{\mu} = 1$.

Because system (2.11) is linear in each region, if a small amplitude periodic solution $p$ exists, the transition plane $\hat{\Sigma}_1$ must divide it in two parts, $p_0$ and $p_1$, belonging to the regions $\hat{S}_{123}$ and $\hat{S}_{23}$, respectively (see Fig. 4). We consider the intersection points $p_0(0)$ and $p_1(0)$, as the initial conditions to solve the system (2.11) in each one of these regions. Thus, we obtain the expressions

$$p_i(t) = e^{N_i t} p_i(0) + \int_0^t e^{N_i s}\, M\, ds, \quad i = 0, 1, \tag{3.1}$$

with $N_0$ and $M$ as in (2.11), and

$$N_1 = \begin{bmatrix} -1 & 0 & 0 \\ -1+\epsilon & -1 & -1-\delta \\ -1-\delta & -1+\epsilon & -1 \end{bmatrix}. \tag{3.2}$$

We assume that $p$ has period $T = T_0 + T_1$, where $T_i$ is the time that the periodic solution expends in the region $\hat{S}_{123}$ and $\hat{S}_{23}$, respectively. Then, the following continuity conditions must be satisfied

$$p_0(T_0) = p_1(0), \quad p_1(T_1) = p_0(0). \tag{3.3}$$

Adding the initial conditions $p_i(0) \in \hat{\Sigma}_1$, for $i = 0, 1$, to the conditions above we obtain a system of eight transcendental equations with eight unknowns: the coordinates of the points $p_i(0)$ and the times $T_i$ for $i = 0, 1$. Solving this system we find the analytical expressions for the periodic solutions of small enough amplitude of (2.3) near the critical value $\mu = c_1$.

Now we consider the critical value $\mu = c_2$, where the boundary equilibrium $\mathbf{x}^* \in \Sigma_2$ was defined in (2.13). Locally, in a neighborhood of the bifurcation, with a suitable change of variables, the system (2.3) can be expressed in the same form of system

(2.11) with

$$N_1 = \begin{bmatrix} -1 & -1-\delta & -1+\epsilon \\ 0 & -1 & 0 \\ -1-\delta & -1+\epsilon & -1 \end{bmatrix}. \tag{3.4}$$

We observe that the unstable focus exists for values of $\mu < c_2$, so in the search for periodic solutions we consider $\hat{\mu} = -1$. The expressions of the two parts of the cycles are defined in (3.1) with the matrix $N_1$ defined in (3.4). Moreover, we consider the continuity conditions given by (3.3) and the initial conditions $p_i(0) \in \hat{\Sigma}_2$, for $i = 0, 1$. Again, we obtain a system of eight transcendental equations. As in the previous case, solving this system we find the expressions of cycles generated in the boundary bifurcation at $\mu = c_2$.

It is important to mention that, in a neighborhood of the boundary equilibrium bifurcation (at the critical values $c_1$ and $c_2$), the scale invariance of (2.11) ensures that the amplitude of the periodic solutions depends linearly on the parameter $\mu$ and their period is constant. This was observed and proved in other piecewise linear neural models [6, 29]. However, if the value of the constant input $\mu$ is far from the critical value, the cycles could show transformations (when they interact with the transition planes) that change their amplitude and period. We consider this situation in the subsection 4.1.

**3.2. Stability of the limit cycles.** Once we found a periodic solution $p$ we can calculate its stability by applying Floquet theory (see, for example, [14, 17]). The linearized equation for the perturbation $\Delta p$ of the cycle results in

$$\frac{d\Delta p}{dt} = J(p(t))\Delta p, \qquad \Delta p(0) = \Delta p_0, \tag{3.5}$$

where $J$ is the Jacobian of the system evaluated along the cycle and $\Delta p_0$ is a small perturbation of $p(0)$. For our system the Jacobian is piecewise constant, the corresponding matrices are $N_0$ or $N_1$ depending on the region, then we obtain the monodromy matrix

$$\Phi(T) = e^{N_1 T_1} e^{N_0 T_0}. \tag{3.6}$$

The eigenvalues of $\Phi(T)$ are the Floquet multipliers. There is always a multiplier equal to 1 associated with the cycle $p$ (see, for example, [14, 17]). If the rest of the multipliers lie inside the unit circle, then the cycle is stable.

We note that for the two critical values of $\mu$ considered in the above section, $\mu = c_1$ and $\mu = c_2$, the difference in the monodromy matrix is given by the matrix $N_1$, defined by (3.2) and (3.4), respectively. Also, we observe that the Floquet multipliers of the cycles with small enough amplitude do not depend on the values of the parameter $\mu$ because the period $T$ of the cycles is constant near the critical values.

**3.3. Existence of limit cycles.** In subsection 3.1 we found that the existence of cycles generated in a boundary equilibrium bifurcation is equivalent to the existence of solutions to certain system of transcendental equations. In this subsection we reduce the dimensionality of this system and prove the existence of solutions by using the Kantorovich theorem for the Newton-Raphson method [26].

We consider the system given by

$$p_0(T_0) = p_1(0), \qquad p_1(T_1) = p_0(0), \qquad p_i(0) \in \Sigma, \quad i = 0, 1, \tag{3.7}$$

where $p_i$ are defined in (3.1) and $\Sigma$ is the transition plane crossed by the cycle ($\hat{\Sigma}_1$ or $\hat{\Sigma}_2$ depending on the considered critical value). As we already mentioned, this system of transcendental equations has eight unknowns: the coordinates of the points $p_i(0)$ and the time values $T_i$, for $i = 0, 1$.

The expressions (3.1) and the continuity conditions allow us to write the following equations

$$e^{N_0 T_0} p_0(0) + \int_0^{T_0} e^{N_0 s} M\, ds = p_1(0), \qquad e^{N_1 T_1} p_1(0) + \int_0^{T_1} e^{N_1 s} M\, ds = p_0(0). \tag{3.8}$$

By replacing $p_0(0)$ on the left for the expression on the right and solving the integrals we obtain the following system of three equations

$$A\, p_1(0) = B, \tag{3.9}$$

where

$$A = (e^{N_0 T_0} e^{N_1 T_1} - I), \tag{3.10}$$

with $I$ the $3 \times 3$ identity matrix, and $B$ is a $3 \times 1$ matrix given by

$$B = e^{N_0 T_0} N_1^{-1} (I - e^{N_1 T_1}) M + N_0^{-1} (I - e^{N_0 T_0}) M. \tag{3.11}$$

Since (3.6) has an eigenvalue equal to 1, $\det(A) = \det\left(e^{N_1 T_1} e^{N_0 T_0} - I\right) = 0$ and the matrix $A$ is non-invertible. Thus, the system (3.9) cannot be solved to find $p_1(0)$, hence we reduce it by considering the initial conditions $p_i(0) \in \Sigma$. Since $p_1(0) \in \Sigma$, we have $n \cdot p_1(0) = 0$, where $n = [n_1, n_2, n_3]$ is normal to the plane $\Sigma$. Thus, by considering $p_1(0) = (\tilde{x}_1, \tilde{x}_2, \tilde{x}_3)$ and $n_3 \neq 0$, we can write the last coordinate $\tilde{x}_3$ as a combination of the first two (here we suppose that $n_3 \neq 0$, if it is not the case, then we change the selection of coordinates on $p_1(0)$). In the new coordinates the system (3.9) results in

$$D \begin{bmatrix} \tilde{x}_1 \\ \tilde{x}_2 \end{bmatrix} = \begin{bmatrix} b_1 \\ b_2 \end{bmatrix}, \tag{3.12}$$

where

$$D = \frac{1}{n_3} \begin{bmatrix} n_3 a_{11} - n_1 a_{13} & n_3 a_{12} - n_2 a_{13} \\ n_3 a_{21} - n_1 a_{23} & n_3 a_{22} - n_2 a_{23} \end{bmatrix}, \tag{3.13}$$

being $a_{ij}$ and $b_i$ the elements of $A$ and $B$ respectively.

The elements in the matrix $A$ depend on the times $T_0$ and $T_1$. For $T_0$ and $T_1$ exist such that $\det(D) \neq 0$, we solve the system (3.12) and find the expressions of the coordinates $\tilde{x}_1(T_0, T_1)$ and $\tilde{x}_2(T_0, T_1)$. Thus, we obtain an expression of the point $p_1(0)$ as a function of $T_0$ and $T_1$.

Now, the condition $p_0(0) \in \Sigma$ can be expressed in the form

$$F_1(T_0, T_1) := n \cdot \left(e^{N_1 T_1} p_1(0) + N_1^{-1} (e^{N_1 T_1} - I) M\right) = 0, \tag{3.14}$$

and the third equation in the system (3.9) yields

$$F_2(T_0, T_1) := [a_{31}, a_{32}, a_{33}] \cdot p_1(0) - b_3 = 0. \tag{3.15}$$

So, we reduce the original system (3.7) to

$$(F_1(T_0,T_1),F_2(T_0,T_1)) = 0. \tag{3.16}$$

A solution to equation (3.16) that satisfies $\det(D) \neq 0$, corresponds to a periodic solution of small enough amplitude for the network (2.3). Despite the low dimensionality of (3.16), its complexity makes it difficult to prove the existence of solutions in the general case. However, one advantage of this system is that its solutions can be interpreted as the intersection of curves in the $(T_0, T_1)$ plane, which allows for a geometric (graphic) study of the system as the parameters vary. Once we find values for the parameters $\delta$ and $\epsilon$ such that (3.16) has a solution, we prove its existence by using the following Kantorovich's convergence result [26].

Let $F : X \to Y$ be an operator, where $X$ and $Y$ are Banach spaces. We consider the recurrent method defined by

$$x_{k+1} = x_k - F'(x_k)^{-1}F(x_k), \qquad k = 0, 1, \ldots, \tag{3.17}$$

where $F'(x_k)$ is the Fréchet derivative of $F(x)$ at the point $x_k$.

THEOREM 3.1 (Kantorovich). *Assume that $F$ is defined and twice continuously differentiable on a ball $B = \{x : \|x-x_0\| \leq r\}$, the linear operator $F'(x_0)$ is invertible, $\|F'(x_0)^{-1}F(x_0)\| \leq \eta$, $\|F'(x_0)^{-1}F''(x)\| \leq K$, $x \in B$, and*

$$h = K\eta < \frac{1}{2}, \qquad r \geq \frac{1-\sqrt{1-2h}}{h}\eta. \tag{3.18}$$

*Then, the equation $F(x) = 0$ has a solution $x^* \in B$, the process (3.17) is well defined and converges to $x^*$ with quadratic rate:*

$$\|x_k - x^*\| \leq \frac{\eta}{h2^k}(2h)^{2^k}.$$

To apply this theorem to our system (3.16), we define the nonlinear operator $F : \mathbb{R}^2 \to \mathbb{R}^2$ as $F(T_0,T_1) = (F_1(T_0,T_1),F_2(T_0,T_1))$. As a first example, we consider the fixed values $\delta = 1/2$ and $\epsilon = 2/5$. We choose the initial value $x_0 = (6, 2.7)$ and the ball $B$ around $x_0$ with ratio $r = 0.25$. Considering the expressions of $F_1$ and $F_2$, we prove that $F$ is twice continuously differentiable on $B$, and that $F'(x_0)$ is invertible. In addition, we have $\|F'(x_0)^{-1}F(x_0)\| \leq \eta = 0.05$ and $\|F'(x_0)^{-1}F''(x)\| \leq K = 8$, for all $x \in B$. Thus, the hypotheses of the theorem are satisfied. This proves the existence of a unique solution $x^*$ of (3.16) in $B$, which could be calculated with the recursive method (3.17) (see Fig. 5 a). Next, we consider $\delta = 1/2$ and $\epsilon = 1/4$, the initial value $x_0 = (6.4, 6.6)$ and the ball $B$ around $x_0$ with radius $r = 0.2$. The operator $F$ is twice continuously differentiable on $B$, and $F'(x_0)$ is invertible. Also, we note that $\|F'(x_0)^{-1}F(x_0)\| \leq \eta = 0.12$ and $\|F'(x_0)^{-1}F''(x)\| \leq K = 3.7$, for all $x \in B$. Thus, we can apply the theorem and prove the existence of a unique solution $x^*$ of (3.16) in $B$ (see Fig. 5 b).

We also note that system (3.16) has no solutions when the parameter $\epsilon$ is below some threshold value $\epsilon^*$ which changes depending on $\delta$. This can be easily seen from a graphical study of (3.16) when the value of $\epsilon$ decreases. In these cases, there are no small amplitude periodic solutions of (2.3) and numeric calculations indicate that all solutions are attracted by an equilibrium of the system ($\mathbf{x}_2^*$ or $\mathbf{x}_3^*$ depending on the considered region). When $\epsilon$ is decreasing and approaching to the threshold value, we see that $T_1$ is increasing and $T_0$ remains near a fixed value. The time $T_1$ spent by the

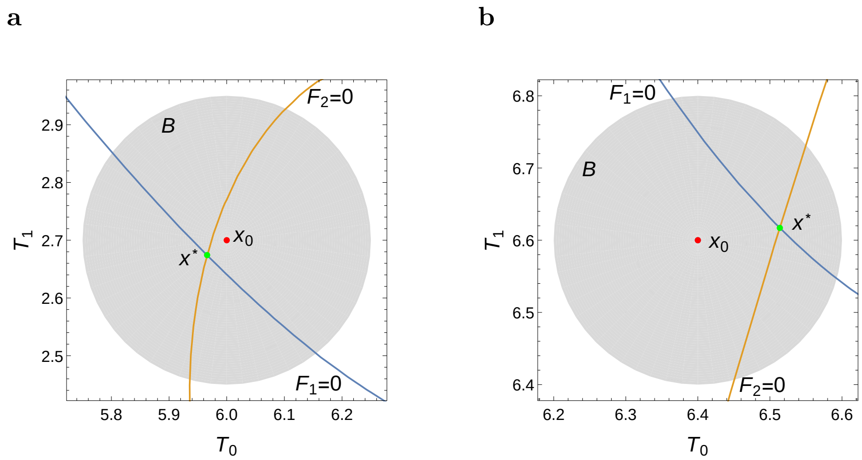


FIG. 5. *Solutions of* (3.16) *for fixed values of the parameters.* **a.** $\delta = 1/2$ *and* $\epsilon = 2/5$. **b.** $\delta = 1/2$ *and* $\epsilon = 1/4$. *The point* $x_0$ *is the initial condition and* $x^*$ *the unique solution on* $B$.

limit cycle trajectory in the region $S_{23}$ grows because this trajectory of the solution is near a stable direction of a saddle equilibrium. We conjecture that these behaviors are connected to the existence of a heteroclinic orbit in the system, but a detailed investigation of this issue is beyond the scope of the present work.

**3.4. Branches of cycles near the equilibrium bifurcations.** For values of the parameter $\mu$ near a boundary equilibrium bifurcation, the existence of a solution to (3.16) implies the existence of a branch of periodic solutions generated in that bifurcation point. These branches exist for non-smooth fold and persistent bifurcations. For the cycles in these branches, the amplitude depends linearly on $\mu$ and the frequency is constant.

For example, we consider the fixed values $\delta = 1/2$ and $\epsilon = 1/4$. The system (2.3) has a non-smooth fold bifurcation at the critical value $\mu = c_1 = 17/24$. We already know that (3.16) has a solution (Fig. 5 b). Now we find a branch of periodic solutions for values of the parameter $\mu > c_1$ and near that critical value. In Figure 6 we show the amplitude of each variable for the cycles in the branch, and the variables as functions of the time for one of these cycles. The period for each cycle in the branch is $T = T_0 + T_1 = 6.5137 + 6.6171 = 13.1308$ and the Floquet multipliers are $\{1., 0.0148303, 9.02392 \times 10^{-16}\}$, thus, the cycles are stable. For the same values of $\delta$ and $\epsilon$, another branch of stable cycles exists for values of the parameter $\mu < c_2 = 22/15$ and near that value (not shown).

**4. Dependence of the limit cycle properties on the model parameters.** As we showed in the above section, limit cycles exist in a neighborhood of the critical values $\mu = c_1$ and $\mu = c_2$. In both cases, the amplitude of the cycles depends linearly on $\mu$ for values near the critical value. But, what is the dependence when the value of the parameter $\mu$ is far from the critical values? In this section we study the attributes (amplitude and period) of the periodic solutions of (2.3) for a large range of values for the parameter $\mu$. In addition, we describe how the connection parameters $\delta$ and $\epsilon$ modify the periodic solutions.

**4.1. Constant input $\mu$.** By increasing (decreasing) the values of $\mu$ from the critical values $c_1$ ($c_2$), a branch of limit cycles is generated and the amplitude of each

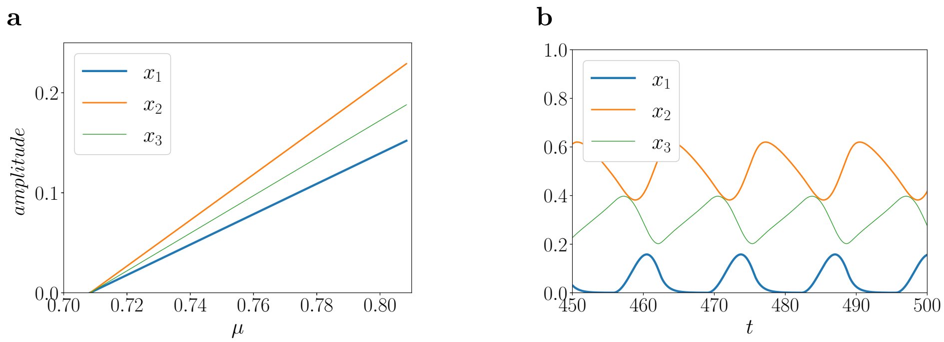


Fig. 6. *Branch of cycles generated in a non-smooth fold bifurcation.* **a.** *Amplitude of each variable as function of the parameter* $\mu$*.* **b.** *Coordinates of the cycle for* $\mu = 0.76$ *as function of* $t$*.*

variable grows until one of the cycles touches tangentially a transition plane different from the one it crossed originally. These contact points are called grazing points [12], next we describe them in the context of our model.

Let $p$ be a periodic solution of (2.3), and let $\Sigma = \{x \in \mathbb{R}^3 : f(x) = 0\}$ be one of the transition planes (defined in (2.6)). The system has a *regular grazing point* in $x_g = p(t_g)$ if $\nabla f(x_g) \neq 0$ and the following conditions are satisfied

$$f(x_g) = 0, \qquad \left.\frac{df(p(t))}{dt}\right|_{t=t_g} = 0, \qquad \left.\frac{d^2 f(p(t))}{dt^2}\right|_{t=t_g} \neq 0. \tag{4.1}$$

The solution $p$ is called a *grazing solution* of the system. The first two conditions in (4.1) ensure that $p$ is tangential to $\Sigma$ in the point $x_g$. The third condition establishes that, in a neighborhood of $t = t_g$, the solution $p$ belongs to one of the regions in $\mathbb{R}^3$ determined by $\Sigma$.

For a given branch of limit cycles generated in a boundary bifurcation, we calculate the *grazing values* $\mu_g$ using the analytical expression of the cycle and the first two conditions in (4.1). Then we check that the third condition is also satisfied. To this end, we calculate the grazing values $\mu_g$ in which a periodic solution of (2.3) has a regular grazing point. Since the calculated points are regular, the cycle does not disappear when the parameter $\mu$ varies. Moreover, it has the same curvature sign near the grazing point for values of the parameter near $\mu_g$. However, both the amplitude and frequency of the cycle are modified after it crosses $\Sigma$, so the grazing values are important to describe them.

As an example, in Figure 7 we show a regular grazing point of a cycle generated in a non-smooth fold bifurcation of (2.3). The situation is also presented in a 2D projection for clarity in the visualization. Originally, the cycle crosses the plane $\Sigma_1$ (Fig. 7 a). As the value of $\mu$ increases we find a grazing point at $\mu = \mu_g$ with the plane $\Sigma_3$ (Fig. 7 b). For values of $\mu > \mu_g$ the cycle crosses $\Sigma_3$ keeping the same curvature sign near the grazing point (Fig. 7 c).

It is important to mention that, by varying the values of $\mu$, the cycles cross different transition planes. For $\mu = 1$ we observe that the limit cycle for system (2.3) is divided into exactly six parts and that it evolves along four regions in the following order: $S_{23} \to S_{123} \to S_{13} \to S_{123} \to S_{12} \to S_{123}$ (see Subsection 6.1 for further details). Heuristically, we observe that for system (2.3) a cycle could be divided in at most six parts, but a proof of this result is beyond the scope of this

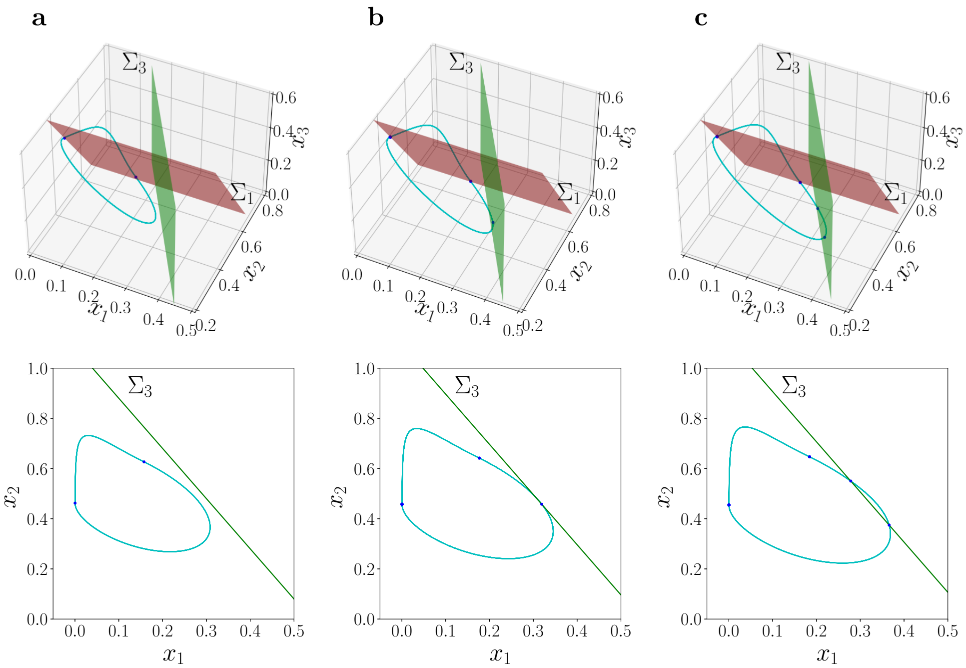


FIG. 7. *Example of grazing point in a periodic solution of* (2.3) *at a grazing critical value* $\mu_g$. *Solution and transition planes in the 3D state space (upper row) and a projection in the* $x_1$-$x_2$ *plane (lower row). Value of the parameter:* **a.** $\mu < \mu_g$. **b.** $\mu = \mu_g$. **c.** $\mu > \mu_g$. *The blue dots indicate the intersection between the periodic solution and the transition planes.*

paper. Regardless of the number of parts in which the cycle is divided, its analytical expression is calculated by applying the same ideas we developed for a cycle with two parts in Subsection 3.1 (by solving the equation in each region and considering continuity conditions). In all cases, by performing the reduction in Subsection 3.3, we obtain a system of transcendental equations that can be numerically solved. To calculate the different grazing values of $\mu$ we add the conditions in (4.1). We calculate the stability of these cycles by adapting the calculations in Subsection 3.2.

In Figure 8 we show the periodic solutions observed in a non-smooth fold case for the indicated values of the parameters. We plot the amplitude of each variable of the cycle (Fig. 8 a) and its frequency (Fig. 8 b) as functions of the input parameter $\mu$. We note that a stable limit cycle is generated in the bifurcation at the critical value $\mu = c_1$, then, it has four regular grazing points when the value of $\mu$ increases, and finally the cycle disappears in the bifurcation at $\mu = c_2$. As we mention, the frequency is constant for values of the parameter near the critical values. For $\mu = 1$ the network has a cyclic symmetry, the activity of the nodes is the same with a translation in time (Fig. 9 b) so the amplitude is the same for each node, furthermore, this particular cycle has the largest frequency of the whole branch. For values of $\mu$ near the critical value, the activity of each node is concentrated around the correspondent unstable fixed point (Fig. 9 a and c). In addition, we observe that the activity of one node is near zero in a big part of the period whereas the other nodes are always active. The amount of input $\mu$ received by the third node ($\mu < 1$ or $\mu > 1$) determines which node remains almost deactivated for a long time (node 1 or node 2, respectively).

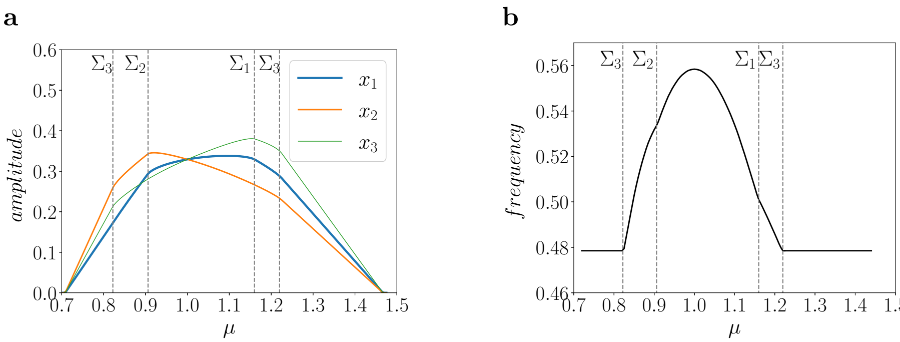


FIG. 8. *Stable periodic solutions of network* (2.3) *varying the parameter* $\mu$ *for the fixed values* $\delta = 1/2$ *and* $\epsilon = 1/4$. **a.** *Amplitude* $((x_{max} - x_{min})/2)$ *of each variable.* **b.** *Frequency of the periodic solutions. The vertical dashed lines correspond to grazing points with the indicated transition planes.*

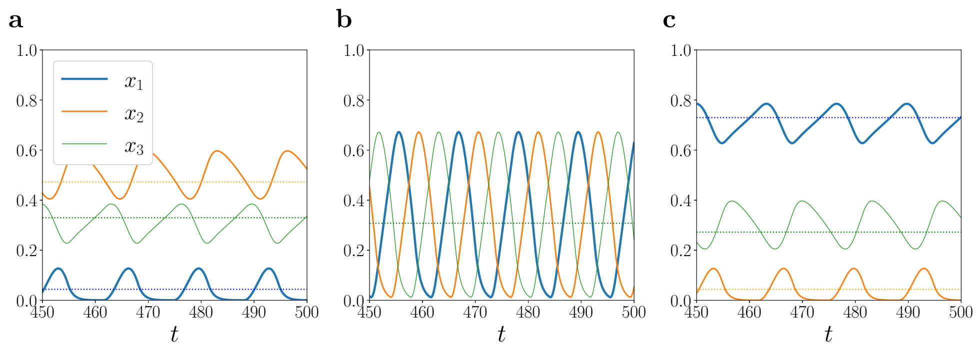


FIG. 9. *Periodic solutions of the network* (2.3) *varying the parameter* $\mu$ *for the fixed values* $\delta = 1/2$ *and* $\epsilon = 1/4$. **a.** $\mu = 0.75$. **b.** $\mu = 1$. **c.** $\mu = 1.4$. *The horizontal dotted lines are the coordinates of the associated unstable focus.*

**4.2. Connection parameters.** In this subsection we consider different values of the connection parameters $\epsilon$ and $\delta$ and show the different limit cycles produced. First we consider a fixed value of $\delta$ and a big range of the $(\mu, \epsilon)$ parameter space, then we vary the value of the parameter $\delta$.

As a representative example we consider $\delta = 1/2$. We obtain similar bifurcation diagrams for other values of $\delta > 0$. For this value of $\delta$ we consider $\epsilon^* < \epsilon < \delta$, with $\epsilon^* \approx 0.159$, since for values of $\epsilon < \epsilon^*$ cycles generated in boundary bifurcations are not found (see Subsection 3.3). In Figure 10 we show the resulting bifurcation diagram. The results regarding the equilibria and their bifurcations were presented in Section 2. For values of the parameter on the left vertical-lined region the unique stable solution of the system is the equilibrium $\mathbf{x}_2^* = [0, 1, 0]^T$ belonging to $S_2$ (see (2.7)), so the node 2 is the only one active in the network. For values on the right vertical-lined region the unique stable solution is the equilibrium $\mathbf{x}_3^* = [0, 0, \mu]^T$ in the region $S_3$, and the node 3 is the only one active. The black curves correspond to the critical values $c_i$, for $i = 1, \ldots, 4$, defined in (2.9). In the shadowed region a stable limit cycle exists, which is generated (destroyed) in the boundary equilibrium bifurcation at $c_1$ on the left ($c_2$ on the right) as the value of $\mu$ increases. For values of the parameters near the black curves the amplitude of the periodic solutions is small

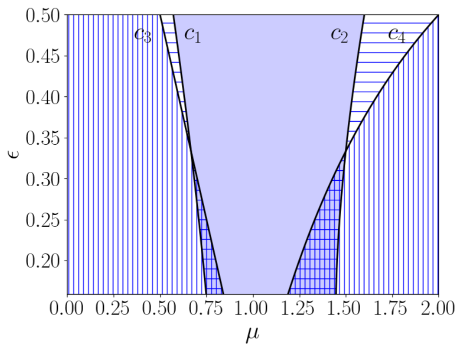


FIG. 10. *Bifurcation diagram of network* (2.3) *for* $\delta = 1/2$. *The black curves indicate the critical values* $c_i$ *where boundary equilibria bifurcation are observed (see* (2.9)*). The left (right) vertical-lined region corresponds to the existence of a stable equilibrium of the network belonging to* $S_2$ *(*$S_3$*) (see* (2.7)*). The left (right) horizontal-lined region corresponds to the existence of a equilibrium of the network belonging to* $S_{23}$ *(*$S_{13}$*). In the upper (lower) horizontal-lined regions the equilibrium is stable (unstable). In the shadowed region the network has a stable limit cycle. In the lined-shadowed regions the network shows multistability.*

and depend linearly on $\mu$ (see Fig. 8). The value $\epsilon_c = \delta/(1+\delta)$ divides the diagram in two parts depending on the type of equilibrium bifurcations. If $\epsilon > \epsilon_c$ the network shows four persistent equilibrium bifurcations when the value of $\mu$ increases, whereas if $\epsilon^* < \epsilon < \epsilon_c$ the network shows four non-smooth fold bifurcations. In the last case, the system shows bistability. There are two regions (lined-shadowed regions) where two stable attractors coexist, an equilibrium ($\mathbf{x}_2^*$ on the left and $\mathbf{x}_3^*$ on the right) and the limit cycle generated in the non-smooth fold bifurcation. We note that the region of multistability is larger for larger values of the constant input $\mu$.

Now, we consider different fixed values of $\mu$, and the connection parameters $\epsilon$ and $\delta$ in a range where stable limit cycles exist (shadowed region in Fig. 10). First, we calculate the frequencies of the cycles (Fig. 11 a and b). We observe that for all values of $\epsilon$ and $\delta$ the largest frequencies are obtained when all the nodes have the same constant input, that is, when $\mu = 1$. Also, we observe that the frequencies increase as the weak inhibition becomes weaker (the value of $\epsilon$ increases), and they tend to the same constant value as $\epsilon$ tends to $\delta$ (Fig. 11 a). In contrast, as the strong inhibition increases (the value of $\delta$ increases), the frequencies increase, reach a maximum and then decrease (Fig. 11 b). Finally, we mention that changes in the weak inhibition affect more the range of frequencies than variations in the strong inhibition. To compare the amplitudes we first consider the case $\mu = 1$. As we already mentioned, for this value of $\mu$ there is a symmetry in the network and the amplitude is the same for each node, we calculate and show this amplitude as a function of the parameters (Fig. 11 c and d). We observe that the amplitude of the symmetric cycle decreases as the weak inhibition becomes weaker, whereas, it slightly decreases and then increases as the strong inhibition becomes stronger. For values of $\mu \neq 1$ some of the amplitude variables increase and others decrease depending on the coordinates of the unstable focus near the trajectory of the solution. However, we observe that, as the (weak or strong) inhibition between nodes is weaker (values of $\epsilon$ increases or values of $\delta$ decreases, respectively), the trajectory of each variable is more uniformly distributed around the coordinates of the unstable focus within a period (Fig. 12).

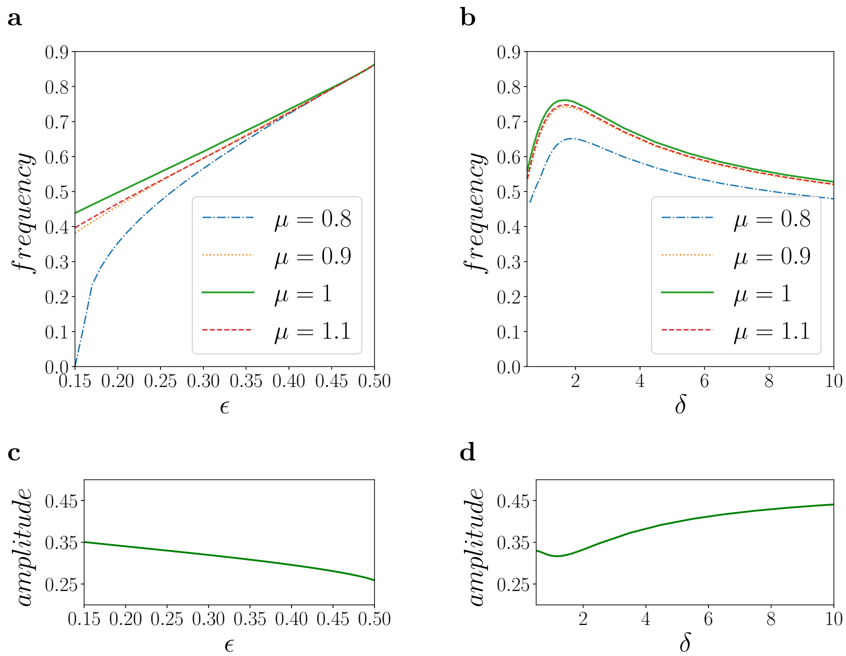


FIG. 11. *Frequencies and amplitudes of periodic solutions of network* (2.3). **a.** *Frequency as function of $\epsilon$ for the indicated values of $\mu$ and $\delta = 1/2$.* **b.** *Frequency as function of $\delta$ for the indicated values of $\mu$ and $\epsilon = 1/4$.* **c.** *Amplitude as function of $\epsilon$ for $\mu = 1$ and $\delta = 1/2$.* **d.** *Amplitude as function of $\delta$ for $\mu = 1$ and $\epsilon = 1/4$.*

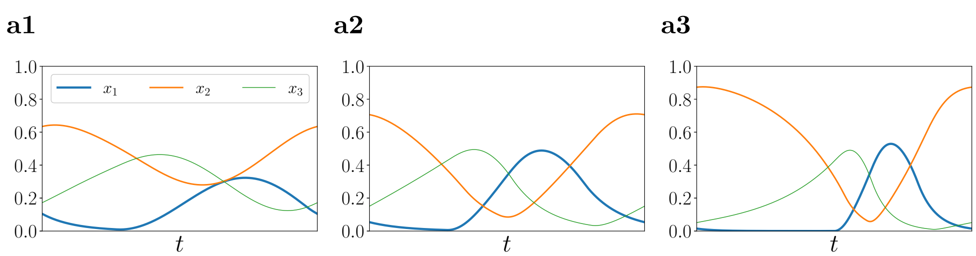


FIG. 12. *Variables for different cycles normalized to one period.* **a1.** *$\delta = 0.5$, $\epsilon = 0.4$ and $\mu = 0.8$.* **a2.** *$\delta = 1$, $\epsilon = 0.4$ and $\mu = 0.8$.* **a3.** *$\delta = 1$, $\epsilon = 0.2$ and $\mu = 0.8$.*

**5. Entrainment of cycles in three-node networks.** In this section we consider a three-node threshold-linear network in the sustained oscillations regime. We assume that an external sinusoidal input is added to one of the nodes and, by defining a Poincaré map, we numerically determine how the input modifies the oscillatory solutions of the network.

We consider the network (2.3) with a sinusoidal input applied to the first node

$$\frac{dx_i}{dt} + x_i = \left[ \sum_{j=1}^{n} W_{ij} x_j + B_i + I_{in,i}(t) \right]_+, \qquad i = 1, 2, 3, \tag{5.1}$$

where $B = [1, 1, \mu]^T$, and the sinusoidal input is given by

$$I_{in,1}(t) = A_{in} \frac{1 + \sin(\omega_{in} t)}{2}, \tag{5.2}$$

where $A_{in}$ is the input amplitude and $\omega_{in}$ is the input frequency, and $I_{in,i}(t) = 0$ for all $i \neq 1$.

The network (5.1) responds to the periodic input with a solution that could be periodic, quasi-periodic or chaotic. If the response is periodic with frequency $\omega_{rsp}$, and the response and input frequencies satisfy $\omega_{rsp}/\omega_{in} = p/q$, for a pair of values $p, q \in \mathbb{N}$, it is said that the network is *entrained* by the input, and the response is a $p : q$ *mode-locked* solution. We study the entrainment regions by considering the Arnold tongues of the network, which are bifurcation diagrams in the parameter space $(\omega_{in}, A_{in})$. The tongue borders correspond to parameter values where cycle bifurcations (such as period doubling and Neimark-Sacker) are observed. For values of the parameter inside the tongues the solutions are synchronized with the input (entrained) with $p : q$ rate. In the rest of the parameter space the solutions are quasi-periodic or chaotic.

The entrainment of oscillatory solutions in neural models for both single oscillators and oscillatory networks has been studied with different mathematical tools, and usually the investigation combines analytical and numerical results [5, 6, 19, 20, 23, 27]. In our model it is possible to obtain systems of transcendental equations for which solutions are in correspondence with points in the tongue borders. These systems are obtained (as in [6]) adding bifurcation conditions to the analytical expressions of the cycles calculated in Section 3. However, the dimension and complexity of these system make them difficult to solve even by using numerical techniques. Because of this, we develop a numerical calculation of the Arnold tongues by defining a Poincaré section and an associated return map to find and describe the mode-locked cycles.

We define the Poincaré section as the plane $x_1 = c^*$, where $c^*$ is the first coordinate of the unstable equilibrium $\mathbf{x}^*_{123}$ for the network without sinusoidal input (see (2.8)). For fixed values of the input parameters ($A_{in}$ and $\omega_{in}$) we calculate the solutions and consider their values for a constant time, large enough to avoid the transitory effect of the initial conditions. To study the return map, we save all times $T_i$ and points $\mathbf{x}(T_i)$ in which the solution crosses the Poincaré section in a selected direction. If the map has a fixed point, i.e., if $\mathbf{x}(T_i)$ is the same for all $i$, and the instant period $T_i - T_{i-1}$ is constant, the solution is a $1 : q$ mode-locked solution. The $q$ value is calculated as the average frequency (approximated by using the instant periods) divided by the input frequency. If the map has a cycle of period two and the instant periods form a sequence of two intercalated values, the network solution is a $2 : q$ mode-locked solution. In general, we extend the above procedure to cycles of period $p$ in the map, to find the $p : q$ mode-locked solutions. In all cases, the $q$ value is calculated as we explained above.

*Remark* 5.1. The proposed calculation of the Arnold tongues is not accurate if the input amplitude is large because of the grazing points that can appear in the solutions. In these cases, for example, a $p : q$ mode-locked solution can be seen as a $1 : q$ mode-locked solution. One option to avoid this problem is consider different Poincaré sections and compare the different Arnold tongues.

**5.1. Results for the three-node network with cyclic symmetry.** Figure 13 shows the Arnold tongues for the three-node network (5.1) with $\mu = 1$ and the values of the connection parameters indicated in the figure. We labeled each region with the $p : q$ type of entrainment. As is expected, each region is expanded from a rational

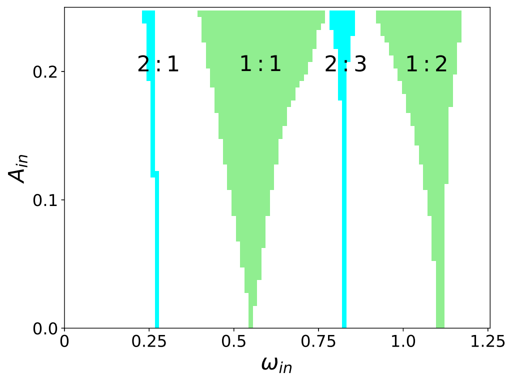


FIG. 13. *Numerical simulations of Arnold tongues for the three node network with sinusoidal input, $\mu = 1$, $\delta = 1/2$ and $\epsilon = 1/4$. The shadowed regions correspond to the different tongues and the labels indicate the $p : q$ type of entrainment. The cycle without input has frequency $\omega \approx 0.553$.*

fraction of the frequency observed without input, and all regions have wedge form, since the entrained solutions are observed for a larger range of the input frequencies when the input amplitude increases. In Figure 14 we show four entrained responses, a $1 : 1$ mode-locked solution (Fig. 14 a), where both the response and input frequencies are the same, and examples of $1 : 2$, $2 : 1$ and $2 : 3$ mode-locked solutions (Figs. 14 b, c and d, respectively). Finally, in Figure 15 we show two quasi-periodic solutions. In this last case, to simplify the visualization, we only show the maximum values for the trajectories of each variable of the cycle.

Now we consider a fixed value of the input amplitude and take a horizontal section of the Arnold tongues. Thus, we can represent a curve in the $(\omega_{in}, \omega_{rps}/\omega_{in})$ space, known as *devil's staircase*, that shows different entrainment regions which correspond to the different Arnold tongues. We show an example (Fig. 16 a) of a devil's staircase obtained for a fixed values of $A_{in}$ and the other parameter values as in Figure 13. To reduce the calculations and compare the response of networks when the connection parameters vary, we calculate different devil's staircases. In particular, we consider three different values of $\epsilon$ (Fig. 16 b). We observe that the entrainment regions are smaller when the weak inhibition is weaker (that is, as the value of $\epsilon$ increases), with exception of the $1 : 1$ region that is slightly larger. In addition, we mention that, as the value of $\epsilon$ is increased, all entrainment regions are obtained for greater values of the input frequency, since the frequency of the network without input is increased.

The Arnold tongues and their devil's staircases contain a lot of information about the response frequency but do not provide us with any information about the response amplitude when the input varies. To analyze this we observe the amplitude of each variable in the $1 : 1$ entrainment region considering two cases, a constant input amplitude $A_{in}$ or a constant input frequency $\omega_{in}$. In the first case, we observed that the response amplitudes are not constant when the value of the input frequency is increased (Fig. 16 a). Moreover, the smallest amplitudes are reached in the largest input frequency, and for the nodes 2 and 3 the amplitudes decrease in the whole range. In the second case (fixed values of the input frequency), the amplitude of the node 1 (receiving the input) is increasing as a function of the input amplitude, and it increases slower as the frequency is closer to the frequency without input (Fig. 16 b). The amplitudes of node 2 and 3 are decreasing, with exception of the amplitude

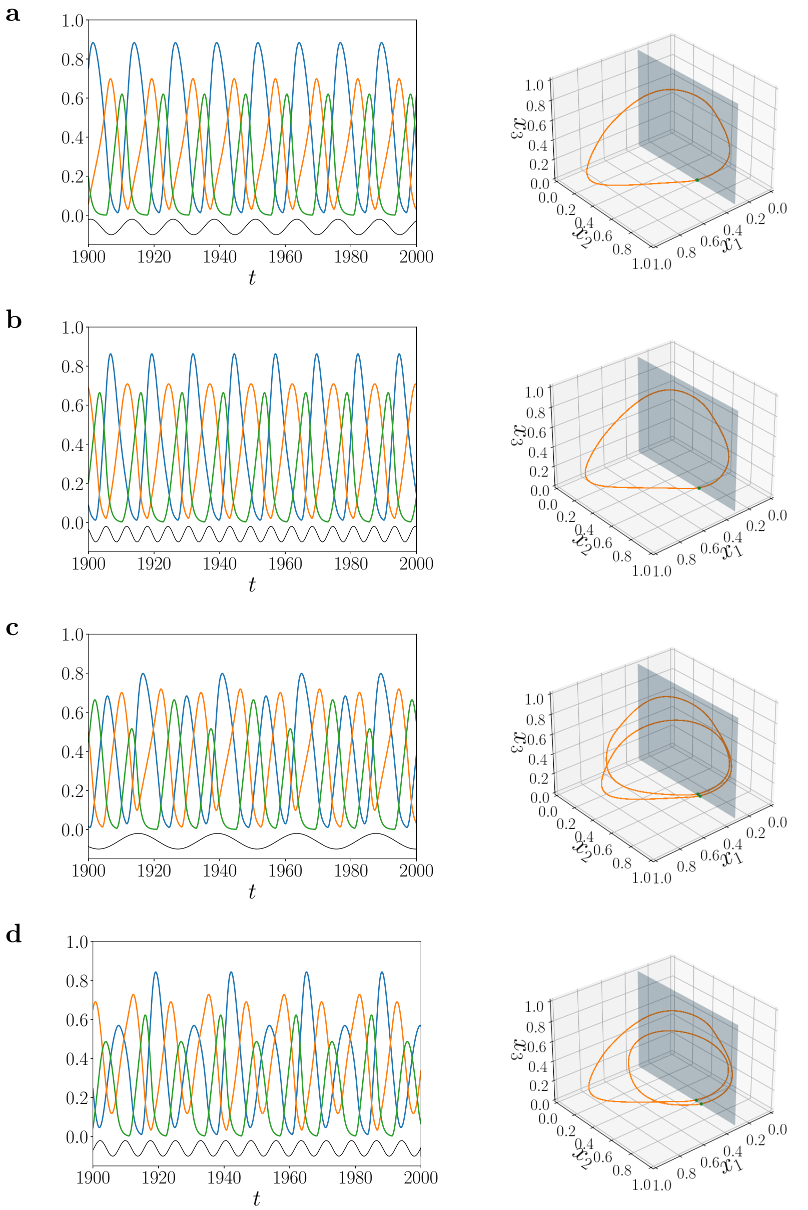


FIG. 14. *Examples of mode-locked cycles for the Arnold tongues in Figure 13. Left column: trajectories as functions of t and a representation of the sinusoidal input (black curve). The input is added to the node one (blue curve). Right column: cycle in the 3D space and its intersections with the Poincaré plane.* **a.** $1:1$ *mode-locked cycle for the input frequency* $\omega_{in} = 0.5$. **b.** $1:2$ *mode-locked cycle for the input frequency* $\omega_{in} = 1$. **c.** $2:1$ *mode-locked cycle for the input frequency* $\omega_{in} = 0.26$. **d.** $2:3$ *mode-locked cycle for the input frequency* $\omega_{in} = 0.82$. *In all cases we consider* $A_{in} = 0.2$, $\mu = 1$, $\delta = 1/2$ *and* $\epsilon = 1/4$.

of node 2 when $\omega_{in}$ is equal to the frequency without input.

To summarize: If the forcing is strong enough, it entrains the network. When the inhibition (weak or strong) between nodes is strong, we observe a large amount

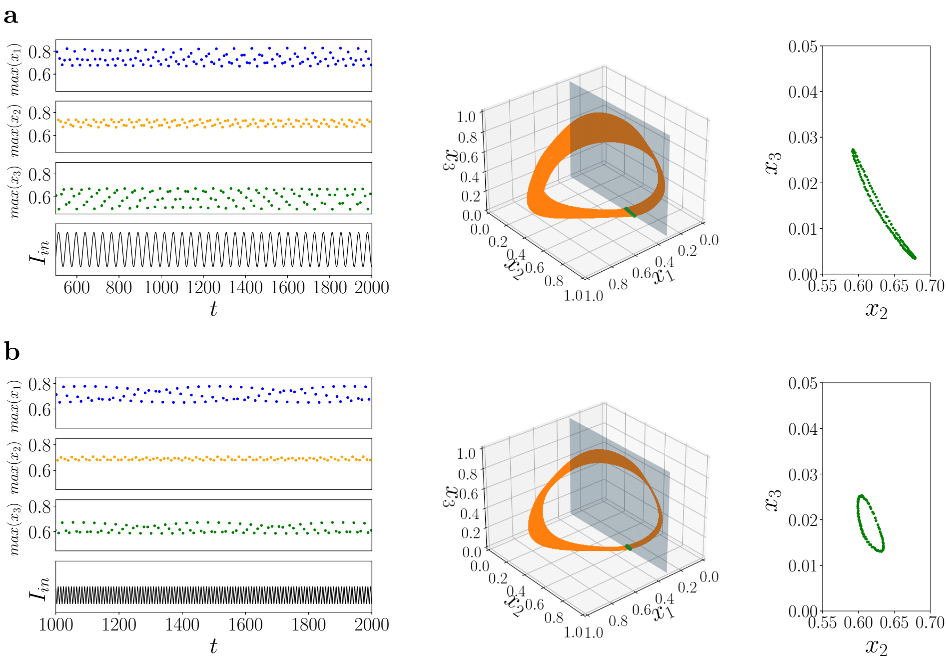


FIG. 15. *Quasi-periodic cycles in the three-node network considered in Figure 13 (for the fixed values $\mu = 1$, $\delta = 1/2$ and $\epsilon = 1/4$). Left column: maximum of each variable as function of $t$. Center column: solution in the 3D space and its intersections with the Poincaré plane. Right column: Poincaré map.* **a.** *Input parameters: $\omega_{in} = 0.15$ and $A_{in} = 0.2$.* **b.** *Input parameters: $\omega_{in} = 0.75$ and $A_{in} = 0.1$.*

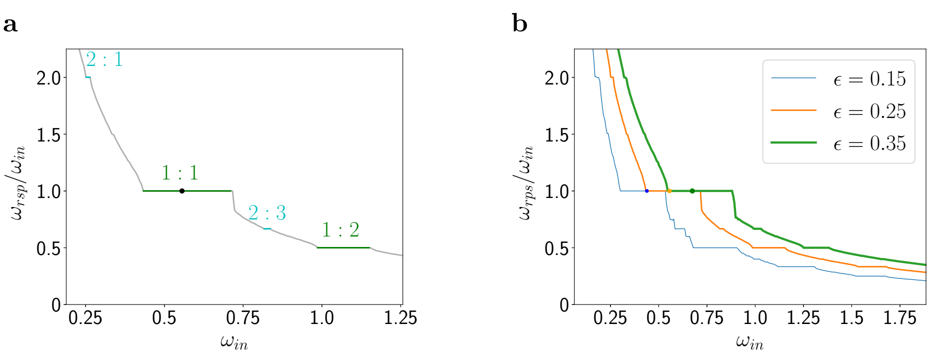


FIG. 16. *Devil's staircase for different three-node networks.* **a.** *Devil's staircase for the fixed values $A_{in} = 0.2$, $\mu = 1$, $\delta = 1/2$ and $\epsilon = 1/4$. We labeled the entrainment regions with the $p : q$ rate of entrainment.* **b.** *Networks for $\mu = 1$, $\delta = 1/2$ and different values of $\epsilon$. The dots indicate the frequency of the periodic solution to the network without input.*

of entrainment regions in a fixed range of frequency inputs. We obtain quasi-periodic solutions if the input is weak or has frequency far from the resonant frequencies.

**6. Cycles in networks with cyclic symmetry and their entrainment.** Here we extend the work developed in the previous sections by studying networks of three or more nodes with all-to-all connections and cyclic symmetry (see Fig. 18).

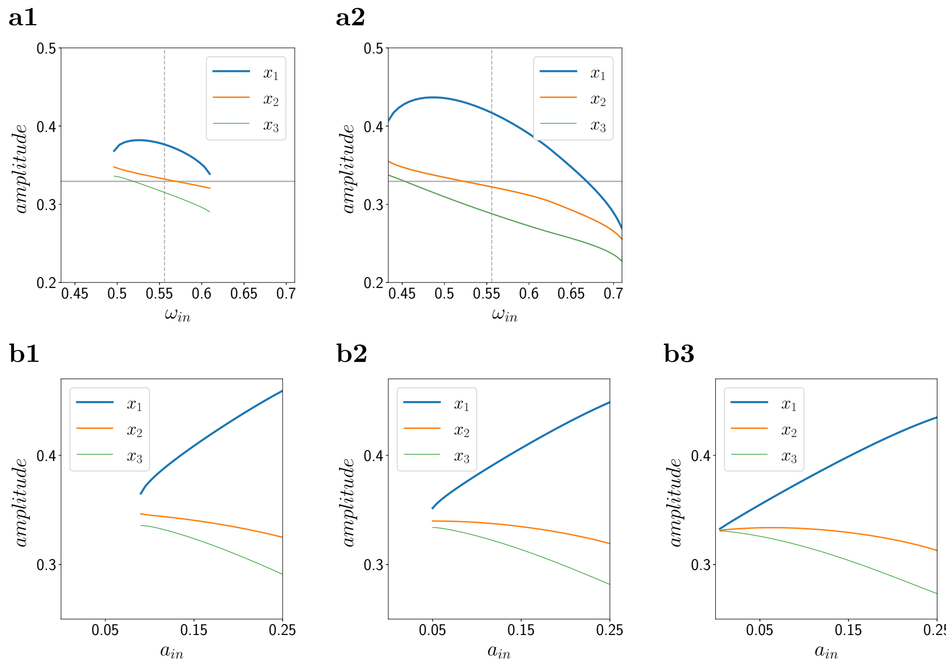


FIG. 17. *Amplitude of each variable for the cycles in the* 1 : 1 *range. We also show the amplitude of the variables without input (horizontal gray line) and frequency without input (vertical dashed line).* **a1.** $A_{in} = 0.1$. **a2.** $A_{in} = 0.2$. **b1.** $\omega_{in} = 0.502$. **b2.** $\omega_{in} = 0.527$. **b3.** $\omega_{in} = 0.553$.

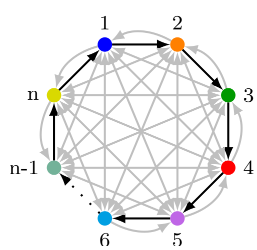


FIG. 18. *Graph representation of a network with* $n$ *nodes and directed connections. A black arrow indicates weak inhibition, whereas a gray arrow indicates strong inhibition between nodes.*

Following the ideas in Section 3, we find the analytical expressions for the oscillatory solutions and obtain a reduced system of two transcendental equations whose solutions correspond to the cycles considered. This leads to extend the proof of the existence of the limit cycles in a straightforward manner. Then, we study the cycle characteristics when the parameter values or the number of nodes vary. Finally, as in Section 5, an external sinusoidal input is added to one of the nodes and we analyze briefly the entrainment of the cycle as the input parameters vary.

**6.1. Cycles in the network of $n$ nodes with all-to-all connections and cyclic symmetry.** The system of differential equations for the threshold-linear network of $n$ nodes with cyclic symmetry is given by

$$\frac{dx_i}{dt} = -x_i + \left[\sum_{j=1}^{n} W_{ij}x_j + \theta_i\right]_+, \qquad i = 1, \dots, n, \tag{6.1}$$

where $W$ is the $n \times n$ matrix given by

$$W = \begin{bmatrix} 0 & -1-\delta & -1-\delta & \dots & -1-\delta & -1+\epsilon \\ -1+\epsilon & 0 & -1-\delta & \dots & -1-\delta & -1-\delta \\ -1-\delta & -1+\epsilon & 0 & \dots & -1-\delta & -1-\delta \\ \vdots & \vdots & \vdots & & & \\ -1-\delta & -1-\delta & -1-\delta & \dots & 0 & -1-\delta \\ -1-\delta & -1-\delta & -1-\delta & \dots & -1+\epsilon & 0 \end{bmatrix}. \tag{6.2}$$

As in the three node case, the values $-1-\delta$ (with $\delta > 0$) and $-1+\epsilon$ (with $0 < \epsilon < 1$) represent the strong and weak inhibitory connections, respectively.

In particular we consider the network with constant input $\theta_i = 1$ in each node. This last assumption generates a cyclic symmetry in the system (already mentioned in the three-node case) from which circular shifts of the nodes does not affect the response of the network.

Following the notation in Section 2, we define

$$f_i(x) = \sum_{j=1}^{n} W_{ij}x_j + 1, \quad \text{and} \quad \Sigma_i = \{x \in \mathbb{R}^n : f_i(x) = 0\}. \tag{6.3}$$

The hyperplanes $\Sigma_i$ divide the state space $\mathbb{R}^n$ in different regions in which the network (6.1) is linear.

The linearity of the system in each region and the symmetry mentioned above allow us to find and calculate periodic solutions applying the techniques developed in Subsection 3.3.

Suppose that a stable limit cycle $p$ of period $T$ exists in the network (6.1). Because of the symmetry in the system, it follows that

$$p_i(t) = p_1\left(t - \frac{i-1}{n}T\right), \qquad i = 2, \dots, n. \tag{6.4}$$

By definition of (6.1), it is necessary that the cycle $p$ crosses at least one transition hyperplane $\Sigma_i$. Then, from condition (6.4) and the definition of $\Sigma_i$, it follows that the cycle crosses all the transition hyperplanes. To find the analytical expression of the cycle, we divide it in $n$ equal parts and study the expression of each coordinate in one interval of length $T/n$ (see Fig. 19 a).

We want to determine which functions $f_i$ are active (have positive values) in each part of the cycle, in order to determine the corresponding linear system (6.1) in each interval. Without loss of generality, in the following calculations we consider the interval $[0, T/n]$ and $p(0) \in \Sigma_1$ (see Fig. 19 b). Thus, $p(T/n) \in \Sigma_2$ and we observe that a value $T_1 \in (0, T/n)$ exists such that

$$p(T_1) \in \begin{cases} \Sigma_1 & \text{if } \ n = 3, \\ \Sigma_4 & \text{if } \ n \geq 4, \end{cases} \tag{6.5}$$

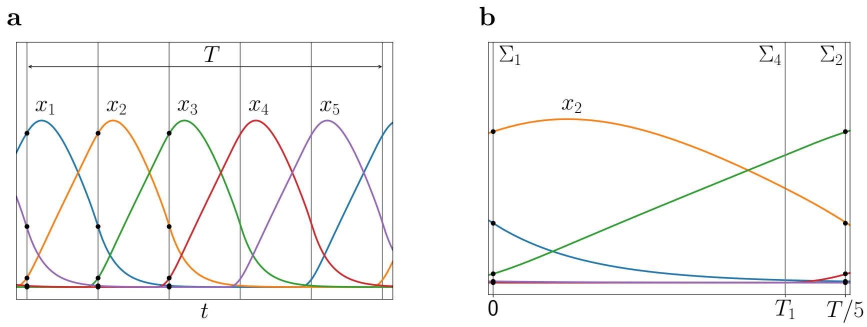


FIG. 19. *Cycle in a network with 5 nodes.* **a.** *Coordinates of the cycle with period $T$. The vertical lines correspond to the transition hyperplanes $\Sigma_i$.* **b.** *Coordinates in an interval of length $T/5$. We consider $p(0) \in \Sigma_1$, so this interval is the second strip in figure* **a**.

and it is satisfied that $f_{2,3}(p(t)) > 0$ for $t \in (0, T_1)$, and

$$\begin{cases} f_{1,2,3}(p(t)) > 0 & \text{if} \quad n = 3, \\ f_{2,3,4}(p(t)) > 0 & \text{if} \quad n \geq 4, \end{cases} \tag{6.6}$$

for $t \in (T_1, T/n)$. Thus, the active functions in the interval $(0, T_1)$ are $f_{2,3}$, whereas in the interval $(T_1, T/n)$ the active functions depend on the value of $n$.

Given the above observations about the signs of the functions $f_i$, we solve system (6.1) in the intervals $(0, T_1)$ and $(T_1, T/n)$ to find the analytical expression of $p$ (as in equation (3.1)). In each interval we solve a linear system of $n$ ordinary differential equations, by considering the initial condition $p(0) \in \Sigma_1$, the continuity condition at $t = T_1$ and the final condition $p(T/n) \in \Sigma_2$. By performing calculations similar to the ones developed in the Subsection 3.3 (where system (3.7) is reduced to (3.16)), we obtain a two dimensional system of transcendental equations with unknowns $T$ and $T_1$. Then, we apply the Kantorovich's result to prove the existence of periodic solutions. Finally, we calculate the stability of $p$ by defining the monodromy matrix following the ideas in Subsection 3.2.

In Figure 19 we show the periodic solution obtained for the network (6.1) with 5 nodes, $\delta = 1/2$ and $\epsilon = 1/4$. In this case, the period is $T = 18.9806$ (and $T_1 = 3.1485$), and the cycle is stable with Floquet multipliers $\{0.99953, 1.32651 \times 10^{-6}, -4.61789 \times 10^{-9} + 1.93239 \times 10^{-8}\mathrm{i}, -4.61789 \times 10^{-9} - 1.93239 \times 10^{-8}\mathrm{i}, 0\}$.

**6.2. Dependence of the oscillatory network dynamics with the model parameters.** In this subsection we briefly study the periodic solution as either the connection parameter $\epsilon$ or the number of nodes vary.

We observe that, for a fixed value of the parameter $\epsilon$, the frequency decreases if the number of nodes increases (Fig. 20 a1). In contrast, for a fixed number of nodes, the frequency increases if the value of $\epsilon$ increases, as in the case of the three-node network considered in the above section.

The amplitude of the cycles in a network having more than three nodes is almost the same as $\epsilon$ changes with some range, and they are always grater than the corresponding amplitude for the three-node case (Fig. 20 a2). In all cases the amplitude decreases as the values of $\epsilon$ increases, i.e., when the weak inhibition becomes weaker, but we observe that the three-node network is more sensitive to this variation.

From the above observations it follows that, for fixed values of the connection

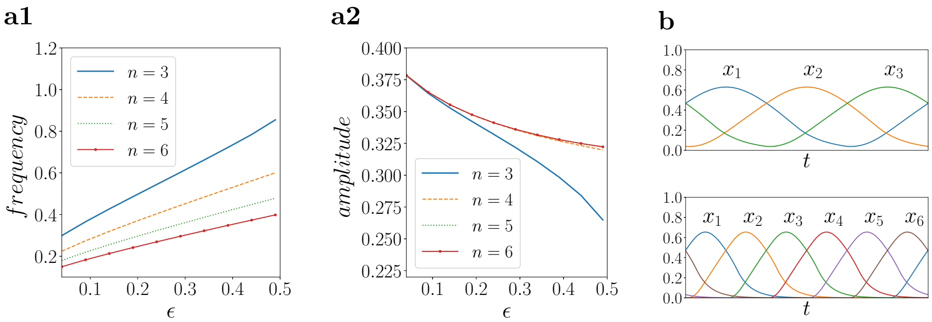


FIG. 20. **a.** *Periodic solutions as functions of $\epsilon$ for the indicated values of $n$ and $\delta = 1/2$.* **a1.** *Frequency.* **a2.** *Amplitude.* **b.** *Variables for different cycles normalized to one period. We consider the fixed values $\delta = 1/2$, $\epsilon = 2/5$ and $n = 3$ ($n = 6$) in the upper (lower) row.*

parameters, as the number of nodes in the network increases the period of the resulting cycle increases.

Finally, we observe that in networks with a large number of nodes, the activity of each one is concentrated near its maximal value and it is near zero for a large amount of time in one period (Fig. 20 b).

**6.3. Entrainment of cycles in networks with cyclic symmetry.** In this subsection we follow the ideas developed in Section 5 and consider the response of the network (6.1) with an oscillatory solution when a periodic input is applied to one of the nodes.

In particular, we consider the network in (6.1) with $n \geq 3$ and $\epsilon < \delta$ (thus the network has a stable limit cycle), and we assume that a positive sinusoidal input is applied to the node labeled as number 1. The resulting system reads

$$\frac{dx_i}{dt} = -x_i + \left[ \sum_{j=1}^{n} W_{ij} x_j + 1 + I_{in,i}(t) \right]_+ , \qquad i = 1, \ldots, n, \tag{6.7}$$

where the input is given by

$$I_{in,1}(t) = A_{in} \frac{1 + \sin(\omega_{in} t)}{2}, \tag{6.8}$$

being $A_{in}$ the input amplitude and $\omega_{in}$ the input frequency, and $I_{in,i}(t) = 0$ for all $i \neq 1$.

We calculate the devil's staircases to compare the response of networks with different number of nodes and values of $\epsilon$. As the number of nodes in the network increases we observe that the entrainment regions become smaller and they shift toward lower frequencies since the frequency without input is smaller for larger number of nodes (Fig. 21 a). This is seen clearly in the 1 : 1 region. Thus, the ability of the input to control the frequency of the response is reduced when the network has a large number of nodes.

For a fixed number of nodes, as we observe for the three-node network (see Fig. 16 b), the entrainment regions shift toward higher frequencies since the frequency without input increases as the value of the connection parameter $\epsilon$ is increased (Fig. 21 b). However, the 1 : 1 entrainment region, which always includes the natural

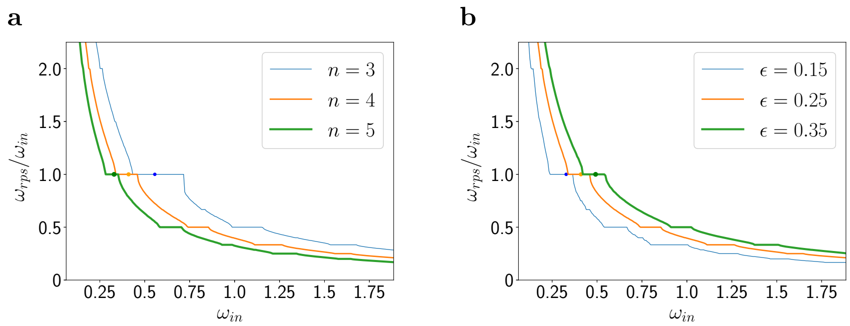


FIG. 21. *Devil's staircases for different networks* (6.7)*.* **a.** *Networks with different number of nodes and fixed the values $\delta = 1/2$ and $\epsilon = 1/4$.* **b.** *Networks with four nodes, $\delta = 1/2$ and the indicated values of $\epsilon$. The dots indicate the frequency of the periodic solution to the network without input.*

frequency (in the absence of any input), does not present big changes in its length. Finally, we note that the network has more entrainment regions in the same interval of input frequencies when the weak inhibition is stronger (lower values of $\epsilon$).

**7. Conclusions.** In this paper we studied the existence of periodic solutions to competitive TLNs and their response to periodic inputs. We first analyzed the three-node case and we later considered networks with three or more nodes, all-to-all connections and cyclic symmetry.

In the three-node network we applied the theory of non-smooth dynamical systems [12, 30] to perform a detailed mathematical analysis of our system. In particular, we calculated and classified all bifurcations of equilibria, which are the basis for the cycle generation analysis that we performed in the Section 3. Because of the specific type of threshold-nonlinearity we dealt with, we were able to find an analytical expression of the periodic solutions and discuss their stability. In addition, by using a combination of mathematical analysis and numerical simulations, we demonstrated the existence of these periodic solutions by considering a reduced system of transcendental equations and using a Kantorovich's convergence result. The existence of these limit cycles has been hypothesized before on the basis of numerical simulations, but to our knowledge no analytical demonstration of the existence of these oscillations has been provided [9, 24, 25].

Once we proved the existence of periodic solutions, we carried out numerical simulations to study the dependence of them on the model parameters. If the values of the inputs to the nodes are close to each other (that is, if the value of $\mu$ is near 1), we observed that periodic solutions exist for a large range of the connection parameters. In contrast, if the inputs are significantly different from each other, the network needs more local excitation (a larger value of $\epsilon$) to generate oscillatory solutions. If all the inputs have the same value, the network has a cyclic symmetry, and a stable periodic solution exists provided that $\epsilon < \delta$. For fixed values of the connection parameters, the frequency of this symmetric cycle is larger than the frequency of cycles for the non-symmetric networks ($\mu \neq 1$). Furthermore, we note that, despite the fact that the values of $\epsilon$ and $\delta$ modify the strength of the inhibitory connections, the attenuation caused by the local excitation (values of $\epsilon$) has a stronger effect over the attributes of the cycles than the local inhibition (values of $\delta$). In other words, the attributes of the periodic solutions are more sensitive to changes in the weak inhibition (see Subsection

4.2). In particular, we observed that (i) the frequency of the cycles increases as the local excitation increases, and (ii) changes in the local excitation affect more the range of observed frequencies than variations in the local inhibition. In addition, in the symmetric networks (with input $\mu = 1$), we observed that the amplitude of the cycle decreases as the local excitation increases, whereas it slightly decreases and then increases as the local inhibition increases.

It is important to mention that all periodic solutions that we found are stable. However, there are two regions in the $\mu$-$\epsilon$ parameter space where the three-node network shows multistability. Two stable attractors coexist: an equilibrium and the limit cycle generated in a boundary equilibrium bifurcation. The region of multistability is larger for larger values of the constant input $\mu$.

An important question associated to oscillatory networks is their ability to follow oscillatory inputs; i.e., to be entrained [5, 6, 19, 20, 23, 27]. In order to address this issue, we analyzed the response of the three-node competitive TLN with an oscillatory solution when a sinusoidal input is added to one of the nodes. We numerically obtained the Arnold tongues of the network and find different entrainment regions as the amplitude and frequency of the input vary. As is expected, each entrainment region is expanded from a rational fraction of the frequency observed without input, and all regions have wedge form, since the entrained solutions are observed for a larger range of the input frequencies when the input amplitude increases. In other words, if the forcing is strong enough, it entrains the network. Quasi-periodic solutions are observed if the input is weak or its frequency is far from the resonant frequencies. As the value of the local excitation increases, we observed that (i) the entrainment regions are smaller, with exception of the 1 : 1 region that is slightly larger, and (ii) all entrainment regions shift toward higher values of the input frequency, since the frequency of the network without input increases. From these observations it follows that as the weak inhibition becomes weaker the amount of input frequencies that generate an mode-locked response becomes smaller.

To extend our results, we considered competitive TLNs with three or more nodes and cyclic symmetry. We applied the techniques developed in Section 3 to find the periodic solutions and calculate their stability. Also, for these networks we analyzed the response to changes in the parameter values, different number of nodes and a sinusoidal input added to one node. The results we obtained by considering changes in the values of the local excitation are similar to the ones described in the three-node case (Section 4), for both the network with and without sinusoidal input. In addition, as the number of nodes in the network increases, the frequency of the cycle decreases, whereas its amplitude remains almost unchanged if the network has more than three nodes. In all cases, the amplitude decreases as the local excitation is increased. Furthermore, the activity of each node in the cycle is near zero for a larger time period as the number of nodes increases. Finally, we added a sinusoidal input to one node and briefly analyzed the network response. The entrainment regions are smaller and they are shifted towards lower frequencies as the number of nodes in the network increases (because the frequency without input is smaller). Thus, the ability of the input to control the frequency of the response is reduced when the network has a large number of nodes. This shrink of the entrainment regions has been observed, for example, in forced chains of neural oscillators [20, 27].

In conclusion, the entrainment regions, in particular the length of the 1 : 1 range, depend more on the size of the network than on the values of the connections parameters. In particular, we observed that the competitive TLNs with a small number of nodes can follow the input frequency for a larger amount of input frequencies than the networks with a large number of nodes. One option to expand the entrainment regions in networks with a large number of nodes is to increase the input amplitude. However, this could generate grazing points capable of destroying the periodic response of the network. Analyzing this requires further research.

A natural extension of our work, which is particularly interesting to us, is to consider the impact of synaptic delay in every connection between nodes. This delay could represent, for example, the distance between nodes or the action of graduated synapses. Some results about synchronized periodic solutions in competitive TLNs with delay were presented in [2]. However a more complete study of periodic solutions to such networks is still needed.

**Acknowledgments.** This work was supported by the Universidad Nacional del Sur grant PGI 24/L113-2019 (AB, RC, WR) and the National Science Foundation grant DMS-1608077 (HGR).

## REFERENCES

[1] M. Arriaga and E. B. Han, *Dedicated hippocampal inhibitory networks for locomotion and immobility*, Journal of Neuroscience, 37 (2017), pp. 9222–9238, https://doi.org/10.1523/JNEUROSCI.1076-17.2017.

[2] A. Bel, R. Cobiaga, and W. Reartes, *Periodic orbits and chaos in nonsmooth delay differential equations*, International Journal of Bifurcation and Chaos, 29 (2019), p. 1950137, https://doi.org/10.1142/S0218127419501372.

[3] D. A. Burke, H. G. Rotstein, and V. A. Alvarez, *Striatal local circuitry: a new framework for lateral inhibition*, Neuron, 96 (2017), pp. 267–284, https://doi.org/10.1016/j.neuron.2017.09.019.

[4] U. Chialva and W. Reartes, *Heteroclinic cycles in a competitive network*, International Journal of Bifurcation and Chaos, 27 (2017), p. 1730044, https://doi.org/10.1142/S0218127417300440.

[5] S. Coombes and P. C. Bressloff, *Mode locking and arnold tongues in integrate-and-fire neural oscillators*, Phys. Rev. E, 60 (1999), pp. 2086–2096, https://doi.org/10.1103/PhysRevE.60.2086. Erratum (2001) Phys Rev E 63:059901.

[6] S. Coombes, R. Thul, and K. Wedgwood, *Nonsmooth dynamics in spiking neuron models*, Physica D: Nonlinear Phenomena, 241 (2012), pp. 2042–2057, https://doi.org/10.1016/j.physd.2011.05.012.

[7] C. Curto, A. Degeratu, and V. Itskov, *Flexible memory networks*, Bulletin of Mathematical Biology, 74 (2012), pp. 590–614, https://doi.org/10.1007/s11538-011-9678-9.

[8] C. Curto, A. Degeratu, and V. Itskov, *Encoding binary neural codes in networks of threshold-linear neurons*, Neural Computation, 25 (2013), pp. 2858–2903, https://doi.org/10.1162/NECO_a_00504.

[9] C. Curto, J. Geneson, and K. Morrison, *Fixed points of competitive threshold-linear networks*, Neural Computation, 31 (2019), pp. 94–155, https://doi.org/10.1162/neco_a_01151. PMID: 30462583.

[10] C. Curto and K. Morrison, *Pattern completion in symmetric threshold-linear networks*, Neural Computation, 28 (2016), pp. 2825–2852, https://doi.org/10.1162/NECO_a_00869. PMID: 27391688.

[11] P. Dayan and L. F. Abbott, *Theoretical Neuroscience: Computational and Mathematical Modeling of Neural Systems*, The MIT Press, 2001.

[12] M. di Bernardo, C. J. Budd, A. R. Champneys, and P. Kowalczyk, *Piecewise-smooth Dynamical Systems.Theory and Applications*, Springer-Verlag, New York, 2008.

[13] G. B. Ermentrout and D. H. Terman, *Mathematical Foundations of Neuroscience*, vol. 35, Springer, 2010.

[14] J. Guckenheimer and P. Holmes, *Nonlinear Oscillations, Dynamical Systems, and Bifurcations of Vector Fields*, vol. 42 of Applied Mathematical Sciences, Springer, 1983.

[15] R. H. R. Hahnloser, H. S. Seung, and J. J. Slotine, *Permitted and forbidden sets in symmetric threshold-linear networks*, Neural Computation, 15 (2003), pp. 621–638, https://doi.org/10.1162/089976603321192103.

[16] R. L. T. Hahnloser, *On the piecewise analysis of networks of linear threshold neurons*, Neural Networks, 11 (1998), pp. 691–697, https://doi.org/10.1016/S0893-6080(98)00012-4.

[17] J. Hale, *Ordinary Differential Equations*, New York: Wiley-Interscience, 1969.

[18] E. C. Y. Ho, M. Strüber, M. Bartos, L. Zhang, and F. K. Skinner, *Inhibitory networks of fast-spiking interneurons generate slow population activities due to excitatory fluctuations and network multistability*, 32 (2012), pp. 9931–9946, https://doi.org/10.1523/JNEUROSCI.5446-11.2012.

[19] J. Keener, F. Hoppensteadt, and J. Rinzel, *Integrate-and-fire models of nerve membrane response to oscillatory input*, SIAM Journal on Applied Mathematics, 41 (1981), pp. 503–517, https://doi.org/10.1137/0141042.

[20] N. Kopell, G. Ermentrout, and T. Williams, *On chains of oscillators forced at one end*, SIAM Journal on Applied Mathematics, 51 (1991), pp. 1397–1417, https://doi.org/10.1137/0151070.

[21] E. Marder and D. Bucher, *Central pattern generators and the control of rhythmic movements*, Current Biology, 11 (2001), pp. R986–996, https://doi.org/10.1016/S0960-9822(01)00581-4.

[22] E. Marder and R. L. Calabrese, *Principles of rhythmic motor pattern generation*, Physiological Reviews, 76 (1996), pp. 687–717, https://doi.org/10.1152/physrev.1996.76.3.687.

[23] N. Massarelli, G. Clapp, K. Hoffman, and T. Kiemel, *Entrainment ranges for chains of forced neural and phase oscillators*, The Journal of Mathematical Neuroscience, 6 (2016), p. 6, https://doi.org/10.1186/s13408-016-0038-9.

[24] K. Morrison and C. Curto, *Chapter 8 - Predicting neural network dynamics via graphical analysis*, in Algebraic and Combinatorial Computational Biology, R. Robeva and M. Macauley, eds., MSE/Mathematics in Science and Engineering, Academic Press, 2019, pp. 241 – 277, https://doi.org/10.1016/B978-0-12-814066-6.00008-8.

[25] K. Morrison, A. Degeratu, V. Itskov, and C. Curto, *Diversity of emergent dynamics in competitive threshold-linear networks: a preliminary report*, arXiv, (2016), p. 12 pp, https://arxiv.org/pdf/1605.04463v1.pdf.

[26] B. T. Polyak, *Newton-Kantorovich method and its global convergence*, Journal of Mathematical Sciences, 133 (2006), pp. 1513–1523, https://doi.org/10.1007/s10958-006-0066-1.

[27] J. P. Previte, N. Sheils, K. A. Hoffman, T. Kiemel, and E. D. Tytell, *Entrainment ranges of forced phase oscillators*, Journal of Mathematical Biology, 62 (2011), pp. 589–603, https://doi.org/10.1007/s00285-010-0348-6.

[28] S. Rich, H. M. Chameh, M. Rafiee, K. Ferguson, F. K. Skinner, and T. A. Valiante, *Inhibitory network bistability explains increased interneuronal activity prior to seizure onset*, Frontiers in Neural Circuits, 13 (2020), p. 81, https://doi.org/10.3389/fncir.2019.00081.

[29] H. G. Rotstein, S. Coombes, and A. M. Gheorghe, *Canard-like explosion of limit cycles in two-dimensional piecewise-linear models of fitzhugh-nagumo type*, SIAM Journal Applied Dynamical Systems, 11 (2012), pp. 135–180, https://doi.org/10.1137/100809866.

[30] D. J. W. Simpson, *Bifurcations in piecewise-smooth continuous systems*, World Scientific, 2010.

[31] M. A. Whittington, R. D. Traub, N. Kopell, G. B. Ermentrout, and E. H. Buhl, *Inhibition-based rhythms: experimental and mathematical observations on network dynamics*, Int J of Psycophysiol, 38 (2000), pp. 315–336, https://doi.org/10.1016/S0167-8760(00)00173-2.

[32] H. R. Wilson and J. D. Cowan, *Excitatory and inhibitory interactions in localized populations of model neurons*, Biophysical Journal, 12 (1972), pp. 1–24, https://doi.org/10.1016/S0006-3495(72)86068-5.